ELSEVIER

Comput. Methods Appl. Mech. Engrg. 190 (2001) 6231–6256

Computer methods in applied mechanics and engineering

www.elsevier.com/locate/cma

Computational optimization of the vortex manufacturing of advanced materials

T.I. Zohdi *

Institut für Baumechanik und Numerische Mechanik, Universität Hannover, Appelstrasse 9A, 30167 Hannover, Germany

Received 2 September 2000

Abstract

A key component to the success of many modern structural designs is the use of materials with microscopically tailored overall properties. One method to obtain desired macroscopic material behavior is by adding microscopic second phase particles to a base material. The macroscopic behavior of the modified base material is the aggregate response of the particles suspended in the matrix binder. In this regard, a relatively standard manufacturing process is the vortex method, whereby loose particulate additives are stirred into a vortex of molten matrix material. In this work a computational strategy is developed to simulate and accelerate the associated trial and error development of tailored dispersed-type materials manufactured with the vortex method. An algorithm is developed to determine optimal geometrical and mechanical properties of microscopic particulate additives in order to modify a homogeneous base matrix sufficiently enough to deliver a prespecified aggregate response. Consistent with what can be manufactured by the vortex method, microstructures composed of randomly distributed aggregates of particles suspended in a binding matrix are considered. A variety of theoretical issues involved in this process are discussed, and three-dimensional examples involving the finite element method are presented.

Keywords: Microstructural optimization; Inverse problems

1. Introduction

It has become relatively common to employ materials with highly complex, *manipulated*, microstructures in modern engineering designs. The microstructures of such materials are tailored to deliver desired macroscopic responses. To an analyst, some important types of materials are (1) dispersed particulate microstructures; (2) continuous fiber microstructures; (3) discontinuous fiber, whisker or elongated-single-crystal microstructures; and (4) fabric woven-braid microstructures. In this work materials formed by a homogeneous matrix embedded with particulate material are considered (case (1), Fig. 1). The material properties of the particles are design parameters that can be controlled. Additionally, the topologies and volume fractions of the particulate material to be added are further controllable design variables. A relatively standard manufacturing process is the vortex method, whereby the loose particulate material is directly added into the molten matrix (Fig. 1). [1] For an overview of this and related processing methods, see [1]. The macroscopic behavior of the modified base material is the aggregate response of the particles suspended in the matrix binder. Specifically, the macroscopic linearly elastic response of the aggregate, $\mathbb{E}^*$, is a (fourth-order tensor) relation between averages, $\langle \boldsymbol{\sigma} \rangle_\Omega = \mathbb{E}^* : \langle \boldsymbol{\epsilon} \rangle_\Omega$, where $\langle \cdot \rangle_\Omega \stackrel{\text{def}}{=} (1/|\Omega|) \int_\Omega \cdot \, d\Omega$, and

* Present address: Department of Mechanical Engineering, 6195 Etcheverry Hall, The University of California, Berkeley, CA 94720-1740, USA. Tel.: +1-510-642-6834; fax: +1-510-642-6163.

E-mail address: zohdi@newton.berkeley.edu (T.I. Zohdi).

[1] Alternatively, the particulate microstructure can also be achieved via controlled heat treatment during solidification.

0045-7825/01/$ - see front matter
PII: S0045-7825(01)00219-5

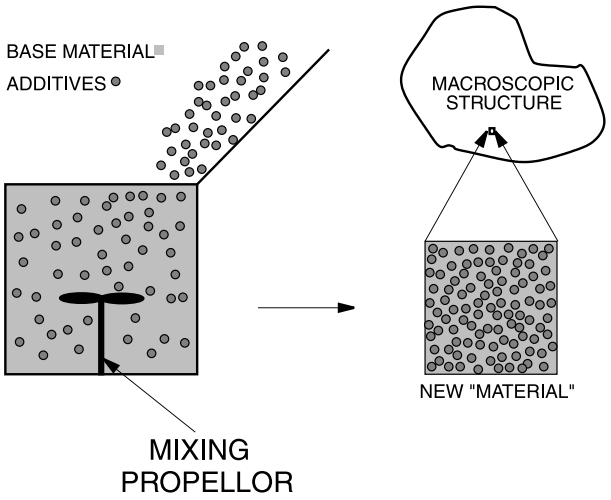

Fig. 1. Doping a material with particulate additives.

where $\boldsymbol{\sigma}$ and $\boldsymbol{\epsilon}$ are the stress and strain tensor fields within a statistically representative volume element (RVE), with volume $|\Omega|$. The effective property is the tensorial parameter used in structural scale computations. It is emphasized that $\mathbb{E}^*$ is not a true material property, but a relation between averages. A more appropriate term might be "apparent property" which is discussed indepth in a series of papers stemming from the materials group at the Ecole Polytechnique Fédérale de Lausanne (EPFL) [2–15]. However, to be consistent with the literature, $\mathbb{E}^*$ will be referred to by the somewhat inaccurate term effective "property".

A commonly accepted macro/micro criterion used in effective property calculations is the so-called Hill condition, $\langle \boldsymbol{\sigma} : \boldsymbol{\epsilon} \rangle_\Omega = \langle \boldsymbol{\sigma} \rangle_\Omega : \langle \boldsymbol{\epsilon} \rangle_\Omega$. Hill's condition dictates the size requirements on the RVE. The classical arguement is as follows. For any perfectly bonded heterogeneous body, in the absence of body forces, two physically important loading states satisfy Hill's condition. They are (1) pure linear boundary displacements of the form $\boldsymbol{u}|_{\partial\Omega} = \mathscr{E} \cdot \boldsymbol{x}$, where

$$\langle \boldsymbol{\epsilon} \rangle_\Omega = \frac{1}{2|\Omega|} \int_\Omega (\nabla \boldsymbol{u} + (\nabla \boldsymbol{u})^{\mathrm{T}}) \, \mathrm{d}\Omega = \frac{1}{2|\Omega|} \int_{\partial\Omega} ((\mathscr{E} \cdot \boldsymbol{x}) \otimes \boldsymbol{n} + \boldsymbol{n} \otimes (\mathscr{E} \cdot \boldsymbol{x})) \, \mathrm{d}A = \mathscr{E}, \tag{1}$$

where $\boldsymbol{u} \otimes \boldsymbol{n} \stackrel{\text{def}}{=} u_i n_j$ is a tensor product of the displacement the vector $\boldsymbol{u}$ and outward unit normal vector $\boldsymbol{n}$, and (2) pure boundary tractions in the form $\boldsymbol{t}|_{\partial\Omega} = \mathscr{L} \cdot \boldsymbol{n}$, where

$$\langle \boldsymbol{\sigma} \rangle_\Omega = \frac{1}{|\Omega|} \int_\Omega \nabla \cdot (\boldsymbol{\sigma} \otimes \boldsymbol{x}) \, \mathrm{d}\Omega = \frac{1}{|\Omega|} \int_{\partial\Omega} (\mathscr{L} \otimes \boldsymbol{x}) \cdot \boldsymbol{n} \, \mathrm{d}A = \mathscr{L}, \tag{2}$$

where $\mathscr{E}$ and $\mathscr{L}$ are constant strain and stress tensors, respectively. Clearly, for Hill's condition to be satisfied within a macroscopic body under nonuniform external loading, the sample must be large enough to possess small boundary field fluctuations relative to its size. Therefore applying (1)- or (2)-type boundary conditions to a large sample is a way of reproducing approximately what may be occurring in a statistically representative mesoscopic subdomain of material within a macroscopic body. Explicitly, to determine $\mathbb{E}^*$, one specifies six linearly independent loadings of the form, (1) $\boldsymbol{u}|_{\partial\Omega} = \mathscr{E}^{(\mathrm{I}\to\mathrm{VI})} \cdot \boldsymbol{x}$ or (2) $\boldsymbol{t}|_{\partial\Omega} = \mathscr{L}^{(\mathrm{I}\to\mathrm{VI})} \cdot \boldsymbol{n}$, where $\mathscr{E}^{(\mathrm{I}\to\mathrm{VI})}$ and $\mathscr{L}^{(\mathrm{I}\to\mathrm{VI})}$ are symmetric second-order strain and stress tensors, with spatially constant components. Each independent loading state provides six equations, for a total of 36, which are used to determine the tensor relation between average stress and strain, $\mathbb{E}^*$. If the effective response is assumed isotropic then only one test loading (instead of usually six), containing nonzero dilatational ($\frac{\mathrm{tr}\,\boldsymbol{\sigma}}{3}$ and $\frac{\mathrm{tr}\,\boldsymbol{\epsilon}}{3}$) and deviatoric components ($\boldsymbol{\sigma}' \stackrel{\text{def}}{=} \boldsymbol{\sigma} - (\mathrm{tr}\,\boldsymbol{\sigma}/3)\boldsymbol{I}$ and $\boldsymbol{\epsilon}' \stackrel{\text{def}}{=} \boldsymbol{\epsilon} - (\mathrm{tr}\,\boldsymbol{\epsilon}/3)\boldsymbol{I}$), is necessary to determine the effective bulk and shear moduli:

$$\boxed{3\kappa^* \stackrel{\text{def}}{=} \frac{\langle \mathrm{tr}\,\boldsymbol{\sigma}/3 \rangle_\Omega}{\langle \mathrm{tr}\,\boldsymbol{\epsilon}/3 \rangle_\Omega} \quad \text{and} \quad 2\mu^* \stackrel{\text{def}}{=} \sqrt{\frac{\langle \boldsymbol{\sigma}' \rangle_\Omega : \langle \boldsymbol{\sigma}' \rangle_\Omega}{\langle \boldsymbol{\epsilon}' \rangle_\Omega : \langle \boldsymbol{\epsilon}' \rangle_\Omega}}.} \tag{3}$$

It is noted that even if the aggregate response is not purely isotropic, one can interpret the above expressions as generalizations of isotropic responses. For overall reviews, the interested reader is referred to [16] for mathematical reviews or to [17–19] for mechanically inclined accounts of the subject.

Within the last 150 years estimates on effective responses have been made under a variety of assumptions on the internal fields of the microstructure. Voigt [20] is usually credited with the first such analysis of the effective mechanical properties of the microheterogeneous solids, with a complementary contribution given later by Reuss [21]. Voigt assumed that the strain field within an aggregate sample of polycrystalline material was uniform, leading to $\langle \mathbb{E} \rangle_{\Omega}$ as an expression of the effective property, while the dual assumption was made by Reuss, who approximated the stress fields within the aggregate of polycrystalline material as uniform. If the Reuss field is assumed within the RVE, then an expression for the effective property is $\langle \mathbb{E}^{-1} \rangle_{\Omega}^{-1}$. A fundamental result [22] is that, under Hill's condition, $\langle \mathbb{E}^{-1} \rangle_{\Omega}^{-1} \leqslant \mathbb{E}^{*} \leqslant \langle \mathbb{E} \rangle_{\Omega}$. These inequalities mean that the eigenvalues of the tensors $\mathbb{E}^{*} - \langle \mathbb{E}^{-1} \rangle_{\Omega}^{-1}$ and $\langle \mathbb{E} \rangle_{\Omega} - \mathbb{E}^{*}$ are nonnegative. Therefore, one can interpret the Voigt and Reuss fields as providing two microfield extremes, since the Voigt stress field is one where the tractions at the phase boundaries cannot be in equilibrium, i.e., statically inadmissible, while the implied Reuss strains are such that the heterogeneities and the matrix could not be perfectly bonded, i.e., kinematically inadmissible. Within the last 50 years improved estimates have been pursued. For example, the *Dilute* family methods assume that there is no particle interaction. With this assumption one requires only the solution to single ellipsoidal particle in an unbounded domain. This is the primary use of the elegant Eshelby [23] formalism, based on eigenstrain concepts, which is used to determine the solution to the problem of a single inclusion embedded in an infinite matrix of material under uniform exterior loading. By itself, this result is of little practical interest, however the solution is relatively compact and easy to use, and thus has been a basis for the development of many approximation methods based on noninteracting and weakly interacting (particle) assumptions. Particulate noninteraction is an unrealistic assumption for materials with randomly dispersed microstructure, even at low volume fractions. Classical attempts to improve the dilute approximations are usually through ideas of "self-consistency" [24,25]. For example, in the standard *self-consistent* method the idea is simply that the particle "sees" the effective medium instead of the matrix in the calculations. In other words the "matrix material" in the Eshelby analysis is simply the effective medium. Unfortunately, the self-consistent method can produce negative effective bulk and shear responses for voids above volume fractions of 50%. For rigid inclusions it produces infinite effective bulk responses for any volume fraction, and infinite effective shear responses for volume fractions above 40%. For details, see [17]. Attempts have also been made to improve these approaches as well. For example the *generalized self-consistent* method encases the particles in a shell of matrix material surrounded by the effective medium (see [26] for details.) However, such methods also exhibit problems, primarily due to mixing scales of information in a phenomenological manner. Such approaches are critically discussed in [27].

Clearly, when dealing with finite sized samples of randomly dispersed matter, most classical assumptions made leading to approximate solutions of micromechanical problems, are not justifiable. Such issues, in particular issues of size effects in (finite) samples, have been discussed indepth in the mentioned papers of the EPFL group. For finite sized samples, numerical simulations are unavoidable. It is now commonly accepted that direct simulations, whereby the macroscopic responses can be obtained by volumetrically averaging (postprocessing) computational micromechanical solutions of aggregate assemblages of material, are beneficial, and can play a complementary role to the laboratory development of new materials. However, such computations are intensive, and it has been only within approximately the last decade, due to the enormous rise in computing power, that such systems could be realistically simulated on single high performance workstations.

In this work a computational strategy is developed to simulate and accelerate the associated trial and error development of tailored dispersed-type materials manufactured when employing the vortex method. An algorithm is developed to determine optimal geometrical and mechanical properties of microscopic particulate additives in order to modify a homogeneous base matrix sufficiently enough to deliver a prespecified aggregate response. Consistent with what can be manufactured by the vortex method, microstructures composed of randomly distributed aggregates of particles suspended in a binding matrix are considered. In order to drive any microstructural design search algorithm, solutions to boundary value formulations posed over the mesoscopic samples of material are required. Algebraic systems of several

thousand numerical degrees of freedom are needed to solve such problems accurately. However, such systems can be routinely simulated on standard high performance workstations, provided that efficient computational techniques are employed. The goal of this work is to develop a microdesign search algorithm with modern desktop computing power and numerical methods implicitly in the background.

Since the finite sized samples considered have random microstructure, there are slight deviations in responses for samples having the same microdesign vector specifications. In other words during a computational (or laboratory) material test, a distribution of $\mathbb{E}^*$'s are obtained, $\mathbb{E}^* \pm \Delta\mathbb{E}^*$, not a single $\mathbb{E}^*$. This macroscopic response "noise" can destroy the ability to construct objective function derivatives, needed for example using a discrete quasi-Newton method. Therefore for each objective function evaluation, for a given microstructural design specification, the responses are averaged over multiple random-microstructure tests. Theoretical characteristics of this regularization process are discussed, and three-dimensional simulations involving the finite element method are presented to illustrate the application of the approach.

The outline of the work is as follows. In Section 2 the design problem is outlined. In Section 3 issues of topological idealization of manufacturable particulate topologies are discussed. In Section 4 the problem of computing reliable numerical derivatives is discussed. In Section 5 numerical simulations are presented. Finally, in Section 6 concluding remarks are given.

2. Microstructural modifications

A structure which occupies an open bounded domain in $\Omega \in \mathbb{R}^3$. Its boundary is denoted $\partial\Omega$ is considered. The body is in static equilibrium under the action of body forces, $\boldsymbol{f}$, and surface tractions, $\boldsymbol{t}$. The boundary $\overline{\partial\Omega} = \overline{\Gamma_u \cup \Gamma_t}$ consists of a part Γ_u and a part Γ_t on which displacements and tractions are respectively prescribed. The mechanical properties of the heterogeneous material are characterized by an elasticity tensor $\mathbb{E} \in \mathbb{R}^{3^2\times 3^2}$ whose components satisfy $\forall \boldsymbol{\epsilon} \in \mathbb{R}^{3\times 3}$, $\boldsymbol{\epsilon} = \boldsymbol{\epsilon}^{\mathrm{T}}$, $a_+\boldsymbol{\epsilon} : \boldsymbol{\epsilon} \geqslant \boldsymbol{\epsilon} : \mathbb{E} : \boldsymbol{\epsilon} \geqslant a_-\boldsymbol{\epsilon} : \boldsymbol{\epsilon}$, $\infty > a_+, a_- > 0$, $\forall \boldsymbol{x} \in \Omega$, where $E_{ijkl} = E_{jikl} = E_{ijlk} = E_{klij}$, $1 \leqslant i,j,k,l \leqslant 3$, and where E_{ijkl} are the Cartesian components of $\mathbb{E}$. The microstructure is assumed to be perfectly bonded. Following standard notation, $H^1(\Omega)$ is denoted as the usual space of functions with generalized partial derivatives of order $\leqslant 1$ in $L^2(\Omega)$. The symbol $\boldsymbol{H}^1(\Omega) \stackrel{\text{def}}{=} [H^1(\Omega)]^3$ is defined as the space of vector-valued functions whose components have generalized partial derivatives $\leqslant 1$ in $\boldsymbol{L}^2(\Omega) \stackrel{\text{def}}{=} [L^2(\Omega)]^3$. The symbol "$\boldsymbol{u}|_{\partial\Omega}$" is used for generalized boundary values, for example for specified boundary displacements.

2.1. A boundary value formulation

A sample of heterogeneous material (Fig. 1), with domain Ω, under a given set of specified boundary loadings, is considered. The variational boundary value problem is

$$\boxed{\begin{array}{l}\text{Find } \boldsymbol{u} \in \boldsymbol{H}^1(\Omega),\ \boldsymbol{u}|_{\Gamma_u} = \boldsymbol{d},\ \text{such that} \\ \quad \int_\Omega \nabla\boldsymbol{v} : \mathbb{E} : \nabla\boldsymbol{u}\,\mathrm{d}\Omega = \int_\Omega \boldsymbol{f}\cdot\boldsymbol{v}\,\mathrm{d}\Omega + \int_{\Gamma_t} \boldsymbol{t}\cdot\boldsymbol{v}\,\mathrm{d}A \quad \forall \boldsymbol{v} \in \boldsymbol{H}^1(\Omega),\ \boldsymbol{v}|_{\Gamma_u} = \boldsymbol{0}.\end{array}} \tag{4}$$

The data are assumed to be such that $\boldsymbol{f} \in \boldsymbol{L}^2(\Omega)$ and $\boldsymbol{t} \in \boldsymbol{L}^2(\Gamma_t)$, but less smooth data can be considered without complications. When material tests satisfying Hill's condition are performed, one has, in the case of displacement controlled tests (loading case (1)) $\Gamma_u = \partial\Omega$ and $\boldsymbol{u}|_{\partial\Omega} = \mathscr{E}\cdot\boldsymbol{x}$ or for traction controlled tests (case (2)) $\Gamma_t = \partial\Omega$ and $\boldsymbol{t}|_{\partial\Omega} = \mathscr{S}\cdot\boldsymbol{n}$. In either case it is considered that $\boldsymbol{f} = \boldsymbol{0}$ and that the material is perfectly bonded. However, it is noted that in case (1) Hill's condition is satisfied with $\boldsymbol{f} = \boldsymbol{0}$ (and no debonding) and in case (2) it is satisfied even with debonding, however only if $\boldsymbol{f} = \boldsymbol{0}$. The boundary value problem in Box 4 must be solved for each new microstructure ($\mathbb{E}$). The solution is then postprocessed for the effective quantities. For the remainder of the work, it is convenient to consider the RVE domain Ω as a cube.

2.2. An objective function

The construction of an objective is straightforward, for example for an isotropic response objective

$$\boxed{\Pi = w_\kappa \left| \frac{\kappa^* - \kappa^{*\mathrm{D}}}{\kappa^{*\mathrm{D}}} \right|^{q_\kappa} + w_\mu \left| \frac{\mu^* - \mu^{*\mathrm{D}}}{\mu^{*\mathrm{D}}} \right|^{q_\mu}}, \tag{5}$$

where κ^* and μ^* are the effective bulk and shear responses produced by a given microstructure, $\kappa^{*\mathrm{D}}$ and $\mu^{*\mathrm{D}}$ are the desired effective bulk and shear responses, w_κ and w_μ are weights, and the q's are positive exponents. Some care must be taken in the choice of the exponents. As an example, consider a one-dimensional bar of length L composed of random particles, i.e., bands in one dimension (Fig. 2). There are a total of N bands, N_2 dark bands, of thickness a, and N_1 the white bands representing the rest. The parameter E_2 represents the "particles", while E_1 represents the "matrix". Suppose one wishes to design an effective response, E^*, of such a structure defined by $\langle \sigma \rangle_\Omega = E^* \langle \epsilon \rangle_\Omega$. Considering uniform strains on the structure and solving the following two-point boundary value problem:

$$\frac{\mathrm{d}}{\mathrm{d}x}\left(E(x)\frac{\mathrm{d}u(x)}{\mathrm{d}x}\right) = 0, \quad u(0) = 0, \quad u(L) = \mathscr{E} \times L,$$

where $\mathscr{E}$ is a constant, one finds that

$$\boxed{E^* = \left\{ 1 \Big/ \left(\frac{(1-v_2)}{E_1} + \frac{v_2}{E_2} \right) \right\} = \underbrace{\langle E^{-1} \rangle_\Omega^{-1}}_{\text{Reuss}} = \frac{E_2}{(1-v_2)\tau_E + v_2}}, \tag{6}$$

where $\tau_E = (E_2/E_1)$, $v_1 + v_2 = 1$ and $v_2 = (N_2 a/L)$. This expression is the same for applied displacement or traction controlled loading, and is exactly the classical Reuss (isostress) bound. This is not surprising since the state of stress is constant throughout the rod, furthermore, $\sigma(x) = \langle \sigma \rangle_\Omega = E^* \langle \epsilon(x) \rangle_\Omega = E^* \mathscr{E}$. Let us focus on two free microstructural variables, the volume fraction of the particles v_2 and E_2, Young's modulus of the particles. It is observed that E^* (Fig. 3) is convex in terms of v_2, and concave in E_2. Consider the following corresponding cost function:

$$\boxed{\Pi = \left| \left(\frac{E_2}{(1-v_2)\tau_E + v_2} - E^{*\mathrm{D}} \right) \Big/ E^{*\mathrm{D}} \right|^q}, \tag{7}$$

where $E^{*\mathrm{D}}$ is the desired effective Young's modulus produced. Fig. 3 shows the trends for the cost function for exponents $q = 0.5$, 1 and 2. Contour plots are also shown. The objective function is rougher, i.e., relatively more nonconvex, for lower values of q. Clearly, values of $q \geqslant 2$ should be chosen to convexify the objective function to a degree that a derivative-based search method, such as a quasi-Newton method, can perform adequately.

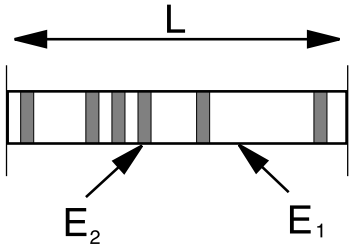

Fig. 2. A one-dimensional structure used to characterize the fundamental objective function structure.

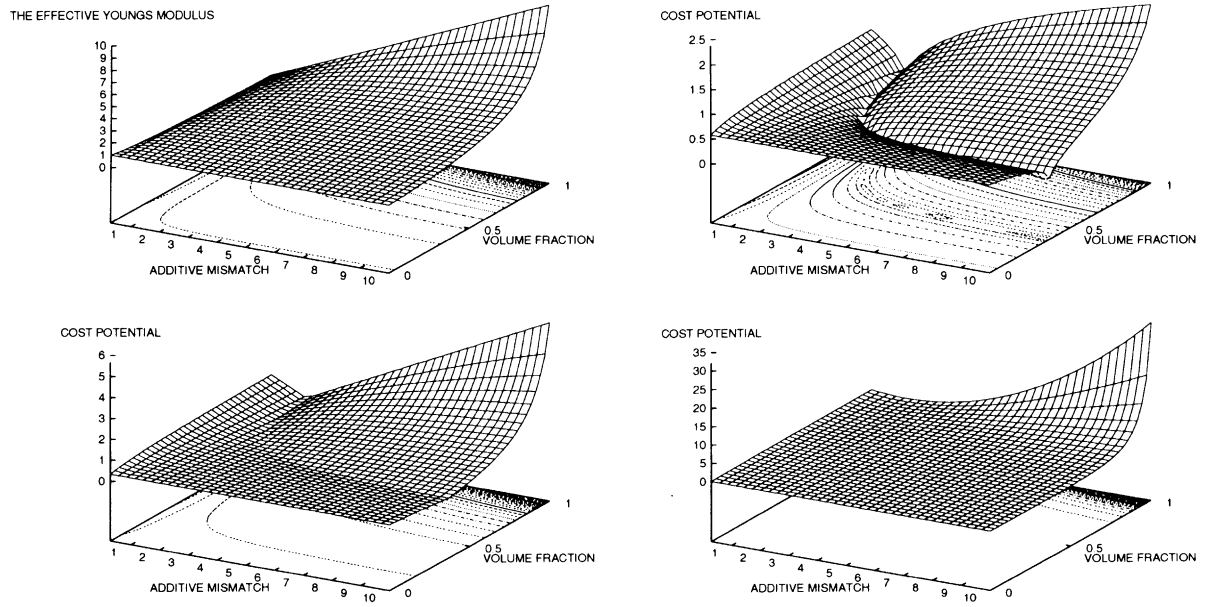

Fig. 3. The effective Young's modulus and objective function for $q = 0.5$, $q = 1.0$, $q = 2.0$.

2.3. Three-dimensional microstructural design parameters

A microstructural design is defined through an N-tuple design vector, denoted $\boldsymbol{\Lambda}$, consisting of the following components: (1) the mechanical properties of the foreign particulate matter; (2) the volume fraction of the foreign particulate matter; (3) the topology of the foreign particulate matter. Ellipsoidal shapes are qualitatively useful since the geometry can mimic a variety of microstructures: (1) platelets when the ellipsoid is oblate with a high aspect ratio; (2) needles or fibers microstructures when it is prolate with high aspect ratio; (3) pores when the particle shapes are spheres with very soft material inside. Accordingly, consider a set of topological microstructural variables which can be conveniently parametrized by a generalized "ellipsoid" (Fig. 4)

$$\boxed{\left(\frac{|x-x_0|}{r_1}\right)^{s_1} + \left(\frac{|y-y_0|}{r_2}\right)^{s_2} + \left(\frac{|z-z_0|}{r_3}\right)^{s_3} = 1,} \tag{8}$$

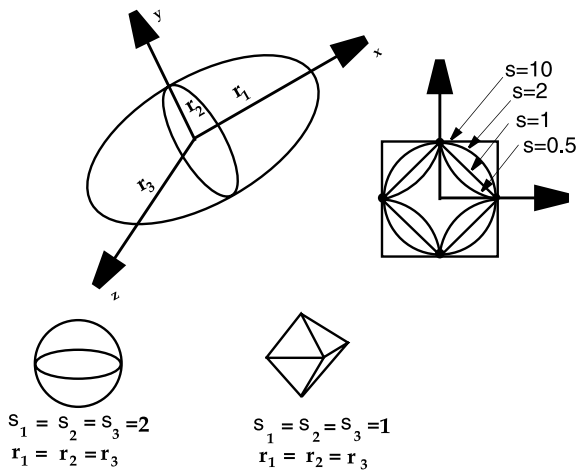

Fig. 4. Parametrization of a generalized ellipsoid.

where the s's are exponents. Values of $s < 1$ produce nonconvex shapes, while $s > 2$ values produce "blocklike" shapes. The following are free variables:

- *Particulate mechanical properties*: assuming local isotropy of the particles, κ_2 and μ_2 (two variables).
- *Polynomial order*: assuming $s_1 = s_2 = s_3 = s$ (one variable).
- *Aspect ratio*: defined by $\mathrm{AR} \stackrel{\mathrm{def}}{=} (r_1/r_2) = (r_1/r_3)$, where $r_2 = r_3$, $\mathrm{AR} > 1$ for prolate geometries and $\mathrm{AR} < 1$ for oblate shapes (one variable).
- *Volume fraction*: via particle/sample size ratio (one variable). This is controlled by defining a subvolume size $V \stackrel{\mathrm{def}}{=} (\{L \times L \times L\}/N)$, where N is the number of particles in the entire sample and where L is the length of the (cubical) sample, $L \times L \times L$. A generalized diameter is defined, δ, which is the diameter of the smallest sphere that can enclose a single particle of possibly nonspherical shape. The ratio between the generalized diameter and the subvolume is one design parameter defined by $\zeta \stackrel{\mathrm{def}}{=} (\delta/V^{\frac{1}{3}})$.

Other design variables, which are not considered in this work, but which could be controlled, include:

- *Matrix mechanical properties*. Assuming local isotropy of the matrix material, κ_1 and μ_1 (two variables).
- *Particulate orientation*. In the last few years, there have been processing methods developed to control the orientation of particulate matter by coating them in a conducting liquid material and introducing them into the molten matrix material (three variables). Thereafter an electrical current is applied, forcing the particles to align themselves along the field lines. This produces globally anisotropic properties.

3. Microgeometrical manufacturing idealizations

Obviously it is virtually impossible to manufacture particles with perfectly smooth geometries. However, if one were to attempt to simulate a sample's response with highly irregular shapes, a problem of such complexity would occur that virtually no analytical, semi-analytical or standard numerical technique would suffice. Fortunately, in the computation of effective properties, the shapes can be safely approximated by much smoother geometrical idealizations, which is the subject of this section.

3.1. Upper and lower variational bounds

Variational inequalities are now derived that govern the growth or decrease in system energy due to the local stiffness reduction. With these inequalities, bounds can be developed for the effective response for irregularly shaped particles by creating outer and inner smooth envelopes, as shown in the Fig. 5. In order to do this the principle of virtual work and the complementary principle are employed.

Consider two symmetric positive definite material property (elasticity tensor) distributions, $\mathbb{E}_{(\mathrm{I})}$ and $\mathbb{E}_{(\mathrm{II})}$ used in same boundary value problem, for example Box 4. The corresponding stress and strain states using these materials are denoted $(\boldsymbol{\epsilon}^{(\mathrm{I})}, \boldsymbol{\sigma}^{(\mathrm{I})})$ and $(\boldsymbol{\epsilon}^{(\mathrm{II})}, \boldsymbol{\sigma}^{(\mathrm{II})})$ respectively. Consider the respective strain energies of both materials:

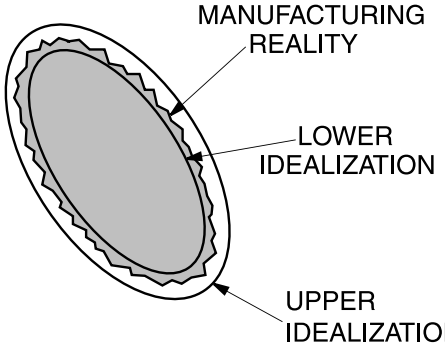

Fig. 5. Upper and lower idealizations of shapes that can be manufactured.

$$W_{\mathrm{I}} \stackrel{\mathrm{def}}{=} \underbrace{\int_{\Omega} \boldsymbol{\epsilon}^{(\mathrm{I})} : \mathbb{E}_{(\mathrm{I})} : \boldsymbol{\epsilon}^{(\mathrm{I})}\, \mathrm{d}\Omega}_{\text{I's energy}} \quad \text{and} \quad W_{\mathrm{II}} \stackrel{\mathrm{def}}{=} \underbrace{\int_{\Omega} (\boldsymbol{\epsilon}^{(\mathrm{I})} + \delta\boldsymbol{\epsilon}) : \mathbb{E}_{(\mathrm{II})} : (\boldsymbol{\epsilon}^{(\mathrm{I})} + \delta\boldsymbol{\epsilon})\, \mathrm{d}\Omega}_{\text{II's energy}}. \tag{9}$$

Denoting $\delta\boldsymbol{\epsilon} = \boldsymbol{\epsilon}^{(\mathrm{II})} - \boldsymbol{\epsilon}^{(\mathrm{I})}$, one obtains

$$\begin{aligned} W_{\mathrm{I}} - W_{\mathrm{II}} &= \int_{\Omega} \boldsymbol{\epsilon}^{(\mathrm{I})} : \mathbb{E}_{(\mathrm{I})} : \boldsymbol{\epsilon}^{(\mathrm{I})}\, \mathrm{d}\Omega - \int_{\Omega} \boldsymbol{\epsilon}^{(\mathrm{I})} : \mathbb{E}_{(\mathrm{II})} : (\boldsymbol{\epsilon}^{(\mathrm{I})} + \delta\boldsymbol{\epsilon})\, \mathrm{d}\Omega - \underbrace{\int_{\Omega} \delta\boldsymbol{\epsilon} : \mathbb{E}_{(\mathrm{II})} : (\boldsymbol{\epsilon}^{(\mathrm{I})} + \delta\boldsymbol{\epsilon})\, \mathrm{d}\Omega}_{=\mathbf{0} \text{ if } \Gamma_u = \partial\Omega} \\ &= \int_{\Omega} \boldsymbol{\epsilon}^{(\mathrm{I})} : (\mathbb{E}_{(\mathrm{I})} - \mathbb{E}_{(\mathrm{II})}) : \boldsymbol{\epsilon}^{(\mathrm{I})}\, \mathrm{d}\Omega - \int_{\Omega} \boldsymbol{\epsilon}^{(\mathrm{I})} : \mathbb{E}_{(\mathrm{II})} : \delta\boldsymbol{\epsilon}\, \mathrm{d}\Omega \\ &= \int_{\Omega} \boldsymbol{\epsilon}^{(\mathrm{I})} : (\mathbb{E}_{(\mathrm{I})} - \mathbb{E}_{(\mathrm{II})}) : \boldsymbol{\epsilon}^{(\mathrm{I})}\, \mathrm{d}\Omega - \underbrace{\int_{\Omega} (\boldsymbol{\epsilon}^{(\mathrm{I})} + \delta\boldsymbol{\epsilon}) : \mathbb{E}_{(\mathrm{II})} : \delta\boldsymbol{\epsilon}\, \mathrm{d}\Omega}_{=\mathbf{0} \text{ if } \Gamma_u = \partial\Omega} + \int_{\Omega} \delta\boldsymbol{\epsilon} : \mathbb{E}_{(\mathrm{II})} : \delta\boldsymbol{\epsilon}\, \mathrm{d}\Omega \\ &= \underbrace{\int_{\Omega} \boldsymbol{\epsilon}^{(\mathrm{I})} : (\mathbb{E}_{(\mathrm{I})} - \mathbb{E}_{(\mathrm{II})}) : \boldsymbol{\epsilon}^{(\mathrm{I})}\, \mathrm{d}\Omega}_{\text{pos. def. when } (\mathbb{E}_{(\mathrm{I})} - \mathbb{E}_{(\mathrm{II})}) > 0 \ \forall \boldsymbol{x}} + \underbrace{\int_{\Omega} \delta\boldsymbol{\epsilon} : \mathbb{E}_{(\mathrm{II})} : \delta\boldsymbol{\epsilon}\, \mathrm{d}\Omega}_{\geqslant 0}. \end{aligned} \tag{10}$$

The vanishing terms in the preceding analysis are due to a direct application of the principle of virtual work. The end result is

$$\boxed{(\mathbb{E}_{(\mathrm{I})} - \mathbb{E}_{(\mathrm{II})}) \geqslant \mathbf{0} \quad \Rightarrow \quad \underbrace{\int_{\Omega} \boldsymbol{\epsilon}^{(\mathrm{I})} : \mathbb{E}_{(\mathrm{I})} : \boldsymbol{\epsilon}^{(\mathrm{I})}\, \mathrm{d}\Omega}_{\text{I's energy}} - \underbrace{\int_{\Omega} (\boldsymbol{\epsilon}^{(\mathrm{I})} + \delta\boldsymbol{\epsilon}) : \mathbb{E}_{(\mathrm{II})} : (\boldsymbol{\epsilon}^{(\mathrm{I})} + \delta\boldsymbol{\epsilon})\, \mathrm{d}\Omega}_{\text{II's energy}} \geqslant 0.} \tag{11}$$

Similarly, defining $\delta\boldsymbol{\sigma} = \boldsymbol{\sigma}^{(\mathrm{II})} - \boldsymbol{\sigma}^{(\mathrm{I})}$, if $\Gamma_t = \partial\Omega$

$$W_{\mathrm{I}} \stackrel{\mathrm{def}}{=} \underbrace{\int_{\Omega} \boldsymbol{\sigma}^{(\mathrm{I})} : \mathbb{E}^{-1}_{(\mathrm{I})} : \boldsymbol{\sigma}^{(\mathrm{I})}\, \mathrm{d}\Omega}_{\text{I's energy}} \quad \text{and} \quad W_{\mathrm{II}} \stackrel{\mathrm{def}}{=} \underbrace{\int_{\Omega} (\boldsymbol{\sigma}^{(\mathrm{I})} + \delta\boldsymbol{\sigma}) : \mathbb{E}^{-1}_{(\mathrm{II})} : (\boldsymbol{\sigma}^{(\mathrm{I})} + \delta\boldsymbol{\sigma})\, \mathrm{d}\Omega}_{\text{II's energy}}, \tag{12}$$

and thus

$$\begin{aligned} W_{\mathrm{I}} - W_{\mathrm{II}} &= \int_{\Omega} \boldsymbol{\sigma}^{(\mathrm{I})} : \mathbb{E}^{-1}_{(\mathrm{I})} : \boldsymbol{\sigma}^{(\mathrm{I})}\, \mathrm{d}\Omega - \int_{\Omega} \boldsymbol{\sigma}^{(\mathrm{I})} : \mathbb{E}^{-1}_{(\mathrm{II})} : (\boldsymbol{\sigma}^{(\mathrm{I})} + \delta\boldsymbol{\sigma})\, \mathrm{d}\Omega + \underbrace{\int_{\Omega} \delta\boldsymbol{\sigma} : \mathbb{E}^{-1}_{(\mathrm{II})} : (\boldsymbol{\sigma}^{(\mathrm{I})} - \delta\boldsymbol{\sigma})\, \mathrm{d}\Omega}_{=\mathbf{0} \text{ if } \Gamma_t = \partial\Omega} \\ &= \int_{\Omega} \boldsymbol{\sigma}^{(\mathrm{I})} : \left(\mathbb{E}^{-1}_{(\mathrm{I})} - \mathbb{E}^{-1}_{(\mathrm{II})}\right) : \boldsymbol{\sigma}^{(\mathrm{I})}\, \mathrm{d}\Omega - \int_{\Omega} \boldsymbol{\sigma}^{(\mathrm{I})} : \mathbb{E}^{-1}_{(\mathrm{II})} : \delta\boldsymbol{\sigma}\, \mathrm{d}\Omega \\ &= \int_{\Omega} \boldsymbol{\sigma}^{(\mathrm{I})} : \left(\mathbb{E}^{-1}_{(\mathrm{I})} - \mathbb{E}^{-1}_{(\mathrm{II})}\right) : \boldsymbol{\sigma}^{(\mathrm{I})}\, \mathrm{d}\Omega + \underbrace{\int_{\Omega} (\boldsymbol{\sigma}^{(\mathrm{I})} + \delta\boldsymbol{\sigma}) : \mathbb{E}^{-1}_{(\mathrm{II})} : \delta\boldsymbol{\sigma}\, \mathrm{d}\Omega}_{=\mathbf{0} \text{ if } \Gamma_t = \partial\Omega} - \int_{\Omega} \delta\boldsymbol{\sigma} : \mathbb{E}^{-1}_{(\mathrm{II})} : \delta\boldsymbol{\sigma}\, \mathrm{d}\Omega \\ &= \underbrace{\int_{\Omega} \boldsymbol{\sigma}^{(\mathrm{I})} : \left(\mathbb{E}^{-1}_{(\mathrm{I})} - \mathbb{E}^{-1}_{(\mathrm{II})}\right) : \boldsymbol{\sigma}^{(\mathrm{I})}\, \mathrm{d}\Omega}_{\text{neg. def. when } (\mathbb{E}^{-1}_{(\mathrm{I})} - \mathbb{E}^{-1}_{(\mathrm{II})}) < 0 \ \forall \boldsymbol{x}} \underbrace{- \int_{\Omega} \delta\boldsymbol{\sigma} : \mathbb{E}^{-1}_{(\mathrm{II})} : \delta\boldsymbol{\sigma}\, \mathrm{d}\Omega}_{\leqslant 0}. \end{aligned} \tag{13}$$

Therefore

$$\boxed{\left(\mathbb{E}^{-1}_{(\mathrm{I})} - \mathbb{E}^{-1}_{(\mathrm{II})}\right) < \mathbf{0} \quad \Rightarrow \quad \underbrace{\int_{\Omega} \boldsymbol{\sigma}^{(\mathrm{I})} : \mathbb{E}^{-1}_{(\mathrm{I})} : \boldsymbol{\sigma}^{(\mathrm{I})}\, \mathrm{d}\Omega}_{\text{I's energy}} - \underbrace{\int_{\Omega} (\boldsymbol{\sigma}^{(\mathrm{I})} + \delta\boldsymbol{\sigma}) : \mathbb{E}^{-1}_{(\mathrm{II})} : (\boldsymbol{\sigma}^{(\mathrm{I})} + \delta\boldsymbol{\sigma})\, \mathrm{d}\Omega}_{\text{II's energy}} \leqslant 0.} \tag{14}$$

3.2. Uses to approximate the effective property

Under the special case of uniform test boundary loadings, one has

$$\boxed{\begin{array}{l}\text{if } \boldsymbol{u}|_{\partial\Omega} = \mathscr{E} : \boldsymbol{x} \quad \text{and} \quad \mathbb{E}_{(\mathrm{I})} - \mathbb{E}_{(\mathrm{II})} \geqslant \mathbf{0} \;\Rightarrow\; 2W_{\mathrm{I}} - 2W_{\mathrm{II}} = \mathscr{E} : \left(\mathbb{E}^{*}_{(\mathrm{I})} - \mathbb{E}^{*}_{(\mathrm{II})}\right) : \mathscr{E}|\Omega| \geqslant 0, \\ \text{if } \boldsymbol{t}|_{\partial\Omega} = \mathscr{L} : \boldsymbol{n} \quad \text{and} \quad \mathbb{E}^{-1}_{(\mathrm{I})} - \mathbb{E}^{-1}_{(\mathrm{II})} \leqslant \mathbf{0} \;\Rightarrow\; 2W_{\mathrm{I}} - 2W_{\mathrm{II}} = \mathscr{L} : \left(\mathbb{E}^{-1*}_{(\mathrm{I})} - \mathbb{E}^{-1*}_{(\mathrm{II})}\right) : \mathscr{L}|\Omega| \leqslant 0.\end{array}} \tag{15}$$

Therefore, if $\mathbb{E}_{(\mathrm{II})}$ is assigned the real microstructure composed of irregular shapes, $\mathbb{E}_{(\mathrm{II})} = \mathbb{E}$, and $\mathbb{E}_{(\mathrm{I})}$ represents a microstructure with a smoother particulate geometry that *envelopes* the real particles (Fig. 5), denoted $\mathbb{E}^{+}$, with corresponding effective property $\mathbb{E}^{*+}$, then $\forall \boldsymbol{x} \in \Omega$ and $\mathbb{E}^{+} - \mathbb{E} \geqslant \mathbf{0}$ or "$\mathbb{E}^{*} \leqslant \mathbb{E}^{*+}$". Alternatively, if $\mathbb{E}_{(\mathrm{I})}$ is assigned the real microstructure composed of irregular shapes, $\mathbb{E}_{(\mathrm{I})} = \mathbb{E}$, and $\mathbb{E}_{(\mathrm{II})}$ represents a microstructure with a smoother particulate geometry that is *enveloped* by the real particles (Fig. 5), denoted $\mathbb{E}^{-}$, with corresponding effective property $\mathbb{E}^{*-}$, then $\forall \boldsymbol{x} \in \Omega$ and $\mathbb{E} - \mathbb{E}^{-} \geqslant \mathbf{0}$ or "$\mathbb{E}^{*-} \leqslant \mathbb{E}^{*}$". Therefore, in total,

$$\boxed{\underbrace{\mathbb{E}^{*-}}_{\text{using inner envelopes}} \leqslant \mathbb{E}^{*} \leqslant \underbrace{\mathbb{E}^{*+}}_{\text{using outer envelopes}}}. \tag{16}$$

To the knowledge of the author, these relations for uniform boundary conditions were first developed in [7,38], based on the results of Hill [28]. The result has been coined by Huet et al. [7] as the "Hill Modification Theorem". Of critical importance is the fact that one can safely use smooth idealizations to approximate rougher more geometrically complicated shapes that really occur during manufacturing.

4. Multi-microvariable searches

For a multi-variate search, to obtain a new directional step for $\boldsymbol{\Lambda}$, $\Delta\boldsymbol{\Lambda}$ is achieved by solving the following system for $\Delta\boldsymbol{\Lambda} \stackrel{\text{def}}{=} (\Delta\Lambda_1, \Delta\Lambda_2, \ldots, \Delta\Lambda_N)$:

$$\begin{bmatrix} \frac{\partial^2 \Pi(\Lambda)}{\partial\Lambda_1\partial\Lambda_1} & \frac{\partial^2 \Pi(\Lambda)}{\partial\Lambda_1\partial\Lambda_2} & \frac{\partial^2 \Pi(\Lambda)}{\partial\Lambda_1\partial\Lambda_3} & \frac{\partial^2 \Pi(\Lambda)}{\partial\Lambda_1\partial\Lambda_4} & \cdots & \cdots \\ \frac{\partial^2 \Pi(\Lambda)}{\partial\Lambda_2\partial\Lambda_1} & \frac{\partial^2 \Pi(\Lambda)}{\partial\Lambda_2\partial\Lambda_2} & \frac{\partial^2 \Pi(\Lambda)}{\partial\Lambda_2\partial\Lambda_3} & \frac{\partial^2 \Pi(\Lambda)}{\partial\Lambda_2\partial\Lambda_4} & \cdots & \cdots \\ \frac{\partial^2 \Pi(\Lambda)}{\partial\Lambda_3\partial\Lambda_1} & \frac{\partial^2 \Pi(\Lambda)}{\partial\Lambda_3\partial\Lambda_2} & \frac{\partial^2 \Pi(\Lambda)}{\partial\Lambda_3\partial\Lambda_3} & \frac{\partial^2 \Pi(\Lambda)}{\partial\Lambda_3\partial\Lambda_4} & \cdots & \cdots \\ \frac{\partial^2 \Pi(\Lambda)}{\partial\Lambda_4\partial\Lambda_1} & \frac{\partial^2 \Pi(\Lambda)}{\partial\Lambda_4\partial\Lambda_2} & \frac{\partial^2 \Pi(\Lambda)}{\partial\Lambda_4\partial\Lambda_3} & \frac{\partial^2 \Pi(\Lambda)}{\partial\Lambda_4\partial\Lambda_4} & \cdots & \cdots \\ \cdots & \cdots & \cdots & \cdots & \cdots & \cdots \\ \cdots & \cdots & \cdots & \cdots & \cdots & \cdots \\ \frac{\partial^2 \Pi(\Lambda)}{\partial\Lambda_N\partial\Lambda_1} & \frac{\partial^2 \Pi(\Lambda)}{\partial\Lambda_N\partial\Lambda_2} & \frac{\partial^2 \Pi(\Lambda)}{\partial\Lambda_N\partial\Lambda_3} & \frac{\partial^2 \Pi(\Lambda)}{\partial\Lambda_N\partial\Lambda_4} & \cdots & \cdots \end{bmatrix} \begin{bmatrix} \Delta\Lambda_1 \\ \Delta\Lambda_2 \\ \Delta\Lambda_3 \\ \Delta\Lambda_4 \\ \cdots \\ \cdots \\ \Delta\Lambda_N \end{bmatrix} = \begin{bmatrix} -\frac{\partial \Pi(\Lambda)}{\partial\Lambda_1} \\ -\frac{\partial \Pi(\Lambda)}{\partial\Lambda_2} \\ -\frac{\partial \Pi(\Lambda)}{\partial\Lambda_3} \\ -\frac{\partial \Pi(\Lambda)}{\partial\Lambda_4} \\ \cdots \\ \cdots \\ -\frac{\partial \Pi(\Lambda)}{\partial\Lambda_N} \end{bmatrix}, \tag{17}$$

or compactly written as $[\mathbb{H}]\{\Delta\boldsymbol{\Lambda}\} = -\{\boldsymbol{g}\}$, where $[\mathbb{H}]$ is the Hessian matrix ($N \times N$), $\{\Delta\boldsymbol{\Lambda}\}$ is the increment ($N \times 1$), and $\{\boldsymbol{g}\}$ is the gradient ($N \times 1$). Central finite difference approximations of the gradient and Hessian components are determined with respect to the material parameters. The finite difference size for the approximate numerical derivatives, different for each component, is denoted h_{Λ_i}. For each variable, the derivative step sizes should be scaled to the size of the current value of that variable, for example $0.05 \times v_2 = h_{v_2}$ or $0.05 \times s = h_s$, etc. The derivatives of the objective function are as follows, using second-order finite difference stencils:

$$\frac{\partial \Pi(\Lambda)}{\partial \Lambda_i} \approx \frac{\Pi(\Lambda_1,\Lambda_2,\ldots,\Lambda_i+h_{\Lambda_i},\ldots,\Lambda_N)-\Pi(\Lambda_1,\Lambda_2,\ldots,\Lambda_i-h_{\Lambda_i},\ldots,\Lambda_N)}{2h_{\Lambda_i}},$$

$$\frac{\partial^2 \Pi(\Lambda)}{\partial \Lambda_i^2} \approx \frac{\Pi(\Lambda_1,\Lambda_2,\ldots,\Lambda_i+h_{\Lambda_i},\ldots,\Lambda_N)-2\Pi(\Lambda_1,\Lambda_2,\ldots,\Lambda_i,\ldots,\Lambda_N)+\Pi(\Lambda_1,\Lambda_2,\ldots,\Lambda_i-h_{\Lambda_i},\ldots,\Lambda_N)}{h_{\Lambda_i}^2},$$

$$\frac{\partial^2 \Pi(\Lambda)}{\partial \Lambda_i \partial \Lambda_j} \approx \frac{\Pi(\Lambda_1,\Lambda_2,\ldots,\Lambda_i+h_{\Lambda_i},\Lambda_j+h_{\Lambda_j},\ldots,\Lambda_N)+\Pi(\Lambda_1,\Lambda_2,\ldots,\Lambda_i-h_{\Lambda_i},\ldots,\Lambda_j-h_{\Lambda_j},\ldots,\Lambda_N)}{4h_{\Lambda_i}h_{\Lambda_j}}$$
$$-\frac{\Pi(\Lambda_1,\Lambda_2,\ldots,\Lambda_i-h_{\Lambda_i},\ldots,\Lambda_j+h_{\Lambda_j},\ldots,\Lambda_N)+\Pi(\Lambda_1,\Lambda_2,\ldots,\Lambda_i+h_{\Lambda_i},\ldots,\Lambda_j-h_{\Lambda_j},\ldots,\Lambda_N)}{4h_{\Lambda_i}h_{\Lambda_j}}. \tag{18}$$

Such relations are used to construct approximations to all components of the gradient and Hessian.

Centrally important is that the *number of objective function evaluations necessary in the problems considered is* $2N^2+1$, where N is the number of microstructural design variables. This stems from the fact that one needs $2(N^2-N)$ objective evaluations for the off-diagonal terms of the Hessian, $2N$ for the diagonal terms, and one evaluation for base point. The total is $2N^2+1$. Therefore even with a small number of design variables the number of objective function evaluations can be quite large. For example with only five variables: (1) the bulk modulus of the additives; (2) the shear modulus of the additives; (3) the volume fraction of the additives; (4) the aspect ratio of the additives; (5) the topology of the additives, one has $2N^2+1=2(25)+1=51$ objective function evaluations per search step. It is clear that, regardless of the microstructure, the construction of the discrete Hessian is the main expense. There exist a variety of "quasi-Newton" methods, which in some manner attempt to approximate the Hessian in an inexpensive way. The approaches, in order of computational expense (cheapest to most expensive) in forming the Hessian are as follows (for N design variables):

- *Level* I: *steepest descent*. $\mathbb{H} \approx \boldsymbol{I}$; number of objective evaluations $= 2N$;
- *Level* II: *diagonal Hessian*. $\mathbb{H} \approx \text{diag}(\mathbb{H})$; number of objective evaluations $= 2N+1$;
- *Level* III: *quasi-Newton*. $\mathbb{H} \approx \text{diag}(\mathbb{H})$ + updates at each iteration. Commonly used updates are for example the Broyden–Fletcher–Golfarb–Shanno (BFGS) updates which require $2N+1$ objective evaluations;
- *Level* IV: *full Newton*. The full Newton construction of the Hessian; number of objective evaluations $= 2N^2+1$.

Remark 1. Level I and Level II require virtually the same amount of work to construct the approximate Hessian, since one must construct the gradient in either case. However, Level II contains more information, and is thus preferred over Level I. Level III methods, which are of the quasi-Newton family, consist of efficient ways of constructing approximate Hessians, i.e., objective function curvature. This is an extremely well-studied topic dating back, at least to the seminal work of Davidon [29] and subsequent improvements by Fletcher and Powell [30]. An exhaustive review of these methods can be found in the well-known texts of Luenberger [34] or Gill et al. [33]. Usually, Level III or IV must be used since there is strong coupling between the microstructural variables. Levels I and II do not capture such effects. Level III is the best option, short of a full (extremely computationally expensive) Newton implementation. For the sake of completeness, the BFGS (Level III) method, which will be used later, is described further in Appendix A.

Remark 2. Another observation is that it is important to scale the design variables to be positive numbers of roughly comparable magnitude. For example, instead of direct mechanical variables one should use property mismatches, i.e., $\tau_\kappa \overset{\text{def}}{=} (\kappa_2/\kappa_1)$ and $\tau_\mu \overset{\text{def}}{=} (\mu_2/\mu_1)$, to avoid dealing with large variations in the design vector components.

4.1. Effective property "noise"

Since the finite sized samples considered have random microstructure, there are slight deviations in responses for samples having the same microdesign vector specifications. In other words during a test a distribution of $\mathbb{E}^*$'s are obtained, $\mathbb{E}^* \pm \Delta\mathbb{E}^*$, not a single $\mathbb{E}^*$. As an example, in order to give an idea of the magnitude of the perturbations, consider an aluminum matrix ($(\kappa, \mu) = (77.9, 24.9$ GPa)) embedded with (stiffening) boron disks ($(\kappa, \mu) = (230, 172$ GPa)). This combination exhibits significant enough mismatch in the mechanical properties to be representative of a wide range of cases, and is a frequently used composite due to its relatively light weight. For the sake of illustration of concepts, the aspect ratio was set to $AR = 0.3$, thus forming oblate "disks" (Fig. 6). A value of $\zeta = 0.75$ was used, which resulted in a volume fraction of approximately 7.7%. The perturbations are shown for 100 different samples (each with 10 disks) in Fig. 7. All tests were run on a single IBM RISC 6000 workstation. Comparable hardware is available in most academic and industrial work places, therefore such simulations are easily reproducible elsewhere for other parameter selections. Throughout the computations a uniform mesh of $20 \times 20 \times 20$ trilinear finite element hexahedra was used (27,783 total degrees of freedom). This corresponds to approximately $9 \times 9 \times 9$ trilinear hexahedra or 2778 numerical dof *per particle*. It has been the experience of the author that such mesh densities (between 2200 and 3000 d.o.f. per particle) deliver stable (mesh independent) results for a wide range of microstructures. During the computations, to increase the resolution of the internal geometry, a "2/5" Gauss rule was applied, whereby a $2 \times 2 \times 2$ Gauss rule if there was no discontinuity in the element, and a $5 \times 5 \times 5$ rule if there was a discontinuity. This process allows for better resolution of the geometry when using uniform

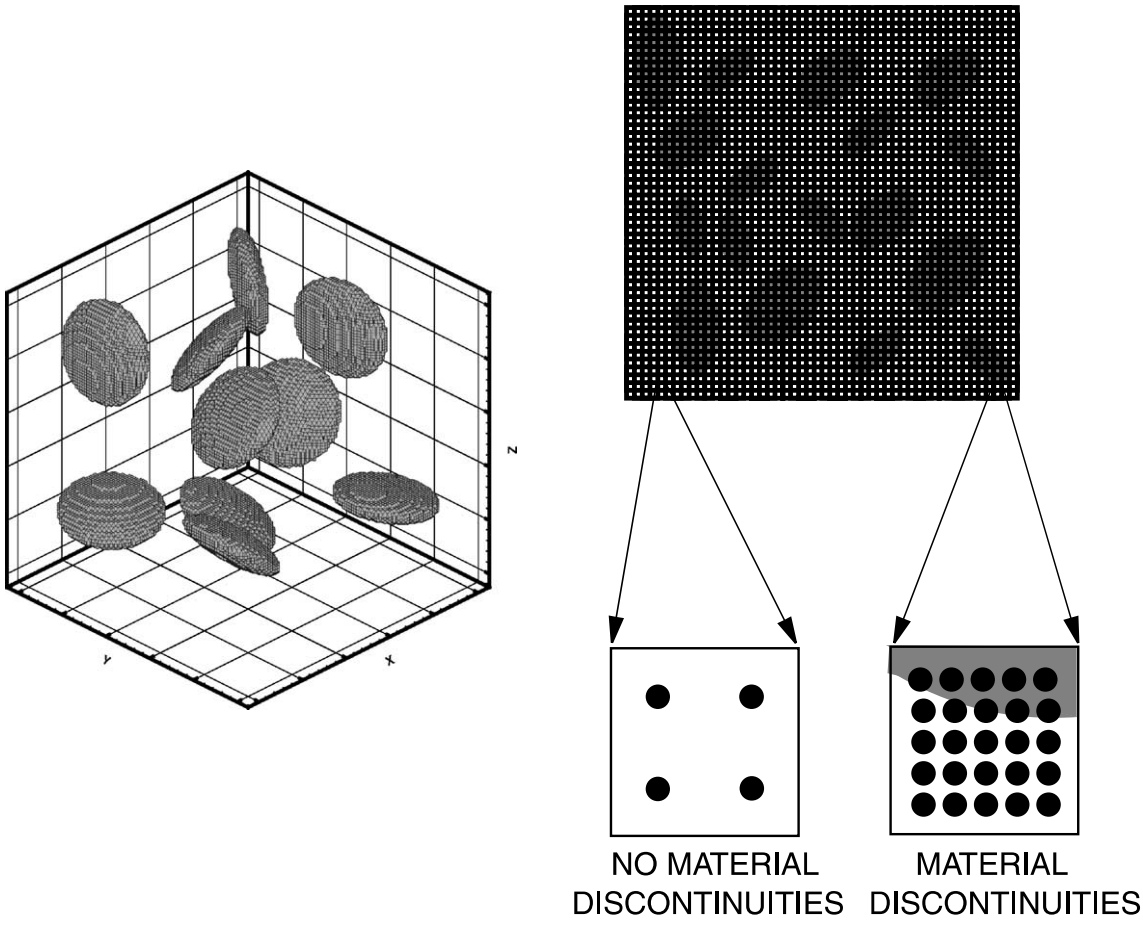

Fig. 6. (Left) The resolved internal geometry of the randomly dispersed disklike particulate material. (Right) A brute force finite element discretization. Elements with material discontinuities have higher Gauss rules applied to capture the geometry within the element. Shown is a cross-section of the mesh density used in the numerical experiments.

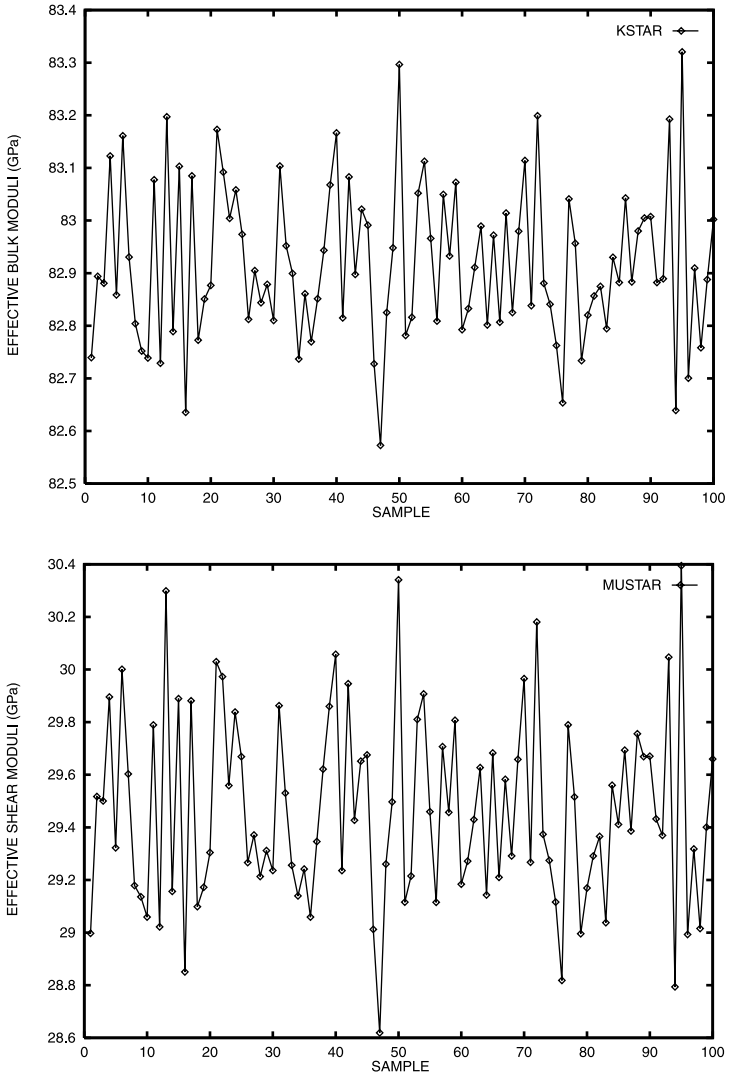

Fig. 7. 100 samples: the effective bulk, κ^*, (top) and shear, μ^*, (bottom) responses, of a block with 10 randomly distributed boron disks embedded in an aluminum matrix.

grids (Fig. 6). The choice of a $5 \times 5 \times 5$ rule is not ad hoc, and has been rigorously proven to deliver under 1% error for the resolution of microstructural topologies in [35].

Displacement controlled tests were considered with $\bar{\mathscr{E}}_{ij} = 0.001$. The effective values, κ^* and μ^*, as defined by Eq. (3) were tracked. The effective modulus, κ^*, exhibits a 1% scatter, while the effective shear modulus, μ^*, a 6% scatter.

Clearly the perturbations (scatter) produced by finite sample sizes can have an effect during the numerical differentiation. As shown in the previous example, this scatter occurs *even at relatively low volume fractions*. For example, take the schematic in Fig. 8. The influence of the sample size in the computation of the derivatives is, where $\mathbb{E}_1^* \overset{\text{def}}{=} \mathbb{E}^*(\boldsymbol{\Lambda})$ and $\mathbb{E}_2^* \overset{\text{def}}{=} \mathbb{E}^*(\boldsymbol{\Lambda} + \Delta\boldsymbol{\Lambda})$,

$$
\begin{aligned}
&\text{one extreme difference} = (\mathbb{E}_2^* + \Delta\mathbb{E}_{2+}^*) - (\mathbb{E}_1^* - \Delta\mathbb{E}_{1-}^*),\\
&\text{other extreme difference} = (\mathbb{E}_2^* - \Delta\mathbb{E}_{2-}^*) - (\mathbb{E}_1^* + \Delta\mathbb{E}_{1+}^*),\\
&\text{difference in extremes} = \Delta\mathbb{E}_{2+}^* + \Delta\mathbb{E}_{2-}^* + \Delta\mathbb{E}_{1+}^* + \Delta\mathbb{E}_{1-}^*,\\
&\text{normalized error} = \frac{\|\Delta\mathbb{E}_{2+}^* + \Delta\mathbb{E}_{2-}^* + \Delta\mathbb{E}_{1+}^* + \Delta\mathbb{E}_{1-}^*\|}{\|\mathbb{E}_2^* - \mathbb{E}_1^*\|}.
\end{aligned}
\tag{19}
$$

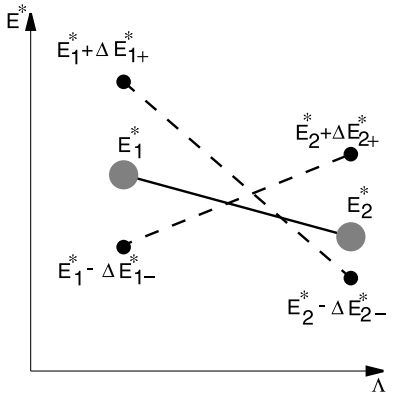

Fig. 8. Effects of the perturbations.

Therefore, the samples must contain a significant amount of microstructure, i.e., they must be relatively large, to compute reliable derivatives. This has been found to be an indispensable ingredient for discrete Newton methods to perform properly, otherwise the gradients oscillate too much, and convergence is questionable. Clearly, the samples and the step sizes in the numerical derivatives have to be sufficiently large so that the difference between effective properties for two neighboring designs is larger than the sum of the size effect perturbations

$$\boxed{\|\Delta\mathbb{E}^*_{2+} + \Delta\mathbb{E}^*_{2-} + \Delta\mathbb{E}^*_{1+} + \Delta\mathbb{E}^*_{1-}\| \ll \|\mathbb{E}^*_2 - \mathbb{E}^*_1\|.} \tag{20}$$

Concisely stated, for accurate numerical derivatives one needs relatively large samples. For example, the 10 particle example considered earlier, is in most likelyhood too rough to allow a Newton scheme to function properly. This is discussed further next.

Remark. Throughout the tests a preconditioned conjugate gradient (PCG) solver was used. This allowed the use of the vector $\boldsymbol{u} = \mathscr{E} \cdot \boldsymbol{x}$, which would be the true "Voigt solution", had the material been homogeneous, as a starting vector to speed up the solution process. This increases the effectiveness of the PCG searches for this class of problems. A well-known fact, with regard to iterative solvers, is that they are quite adept at capturing high frequency responses. However, they typically may require many iterations to capture "long-wave" modes. In other words, a starting vector that captures a-priori the "long wave" components (low frequency eigenmodes) is advantageous. This is obtained by using the Voigt solution as a first guess. For further details see [35]. Typically, for this sample size, a single test took no more that 30 s, therefore 100 tests lasted under 1 h.

4.2. Statistical regularization

In addition to using large samples of material, if one takes the average of multiple tests before constructing the gradients, the results can be further stabilized. Typically, depending on the microstructure, stabilization occurs with under approximately 20 samples. The exact number of tests is controlled by the types of statistical distribution. One can describe the essential characteristics of distributions through statistical moments. Consider a tested quantity, Q, with a distribution of values (Q_i, $i = 1, 2, \ldots, S =$ samples) about an arbitrary reference point, denoted $Q^\star$, as follows:

$$\boxed{\boldsymbol{M}_r^{Q_i - Q^\star} \stackrel{\text{def}}{=} \frac{\sum_{i=1}^{S} (Q_i - Q^\star)^r}{S} \stackrel{\text{def}}{=} \overline{(Q_i - Q^\star)^r},} \tag{21}$$

where $(\sum_{i=1}^{S}(\cdot)/S) \stackrel{\text{def}}{=} \overline{(\cdot)}$ and $\Theta \stackrel{\text{def}}{=} \overline{Q_i}$. The various moments characterize the distribution, for example (1) $\boldsymbol{M}_1^{Q_i - \Theta}$ measures the first deviation from the average, which equals zero; (2) $\boldsymbol{M}_1^{Q_i - 0}$ is the average; (3) $\boldsymbol{M}_2^{Q_i - \Theta}$

is the standard deviation; (4) $\boldsymbol{M}_3^{Q_i-\Theta}$ is the skewness; (5) $\boldsymbol{M}_4^{Q_i-\Theta}$ is the kurtosis. The higher moments, such as the skewness measure the bias, or asymmetry of the distribution of data, while the kurtosis measures the degree of peakedness of the distribution of data around the average. The skewness is zero for symmetric data. Convenient dimensionless measures for these characteristics are defined through

$$\boxed{m_r^{Q_i-\Theta} = \frac{\boldsymbol{M}_r^{Q_i-\Theta}}{\left(\sqrt{\boldsymbol{M}_2^{Q_i-\Theta}}\right)^r},} \tag{22}$$

where (1) $m_1^{Q_i-\Theta} = 0$; (2) $m_2^{Q_i-\Theta} = 1$; (3) $m_3^{Q_i-\Theta} = 0$ for symmetric data; (4) $m_4^{Q_i-\Theta} = 3$ for a "normal" Gaussian distribution; (5) $m_4^{Q_i-\Theta} > 3$ for more peaked than Gaussian distribution (Leptokurtic); (6) $m_4^{Q_i-\Theta} < 3$ for flatter than Gaussian distribution (Platykurtic). For example, for the sample containing 10 disks, the values are shown in Table 1, and indicate that the distribution is sub-Gaussian, i.e., Platykurtic. Larger samples are needed for Gaussian distributions. The author's experience has been that roughly 20 particles per sample attains Gaussian distributions over a wide range of microstructures [35].

Remark. It is advantageous to adaptively compute the average. The most straightforward way to achieve this is to compute the sequential change in the average as more and more samples are tested ($i = 1, 2, 3, \ldots, S$), until the difference in successive terms in the sequence case are less than a tolerance

$$\boxed{\left| \tfrac{1}{S+1} \sum_{i=1}^{S+1} \Pi^{(i)} - \tfrac{1}{S} \sum_{i=1}^{S} \Pi^{(i)} \right| \leq \mathrm{TOL}_A \left| \tfrac{1}{S+1} \sum_{i=1}^{S+1} \Pi^{(i)} \right|.} \tag{23}$$

Adaptively selecting the number of samples needed to stabilize the results is extremely important for two main reasons: (1) it is impossible to know a priori how many samples to test for the average to stabilize and (2) it more cost effective than simply taking a large (overkill) number of samples. The procedure results in different numbers of tested samples for each microstructural vector. Some important sampling theorems indicate that this can be interpreted as testing conglomerated samples of different sizes, which is discussed next.

4.3. Properties of the statistical regularization

Consider the following process for a sample of material with $\boldsymbol{u}|_{\partial\Omega} = \mathscr{E} \cdot \boldsymbol{x}$:

- *Step* 1. Take a large sample, and cut it into S pieces, $\Omega = \bigcup_{K=1}^{S} \Omega_K$. The pieces do not have to be the same size or shape, although for illustration purposes it is convenient to take a uniform (regular) partitioning (Fig. 9)
- *Step* 2. Test each piece (solve the subdomain BVP) with the loading: $\boldsymbol{u}|_{\partial\Omega_K} = \mathscr{E} \cdot \boldsymbol{x}$. The function $\tilde{\boldsymbol{u}}_K$ is the solution to the BVP posed over subsample Ω_K
- *Step* 3. One is guaranteed the following properties:

$$\boxed{\begin{array}{l} \langle \tilde{\boldsymbol{\sigma}} \rangle_{\Omega_K} \overset{\text{def}}{=} \tilde{\mathbb{E}}_K^* : \langle \tilde{\boldsymbol{\epsilon}} \rangle_{\Omega_K}, \quad \tilde{\mathbb{E}}^* \overset{\text{def}}{=} \sum_{K=1}^{S} \tilde{\mathbb{E}}_K^* \frac{|\Omega_K|}{|\Omega|}, \\ \|\boldsymbol{u} - \tilde{\boldsymbol{u}}\|_{E(\Omega)}^2 = \mathscr{E} : (\tilde{\mathbb{E}}^* - \mathbb{E}^*) : \mathscr{E}|\Omega| \leqslant \mathscr{E} : (\tilde{\mathbb{E}}^* - \langle \mathbb{E}^{-1} \rangle_{\Omega}^{-1}) : \mathscr{E}|\Omega|, \\ \langle \mathbb{E}^{-1} \rangle_{\Omega}^{-1} \leqslant \mathbb{E}^* \leqslant \tilde{\mathbb{E}}^* \leqslant \langle \mathbb{E} \rangle_{\Omega}, \\ \tilde{\boldsymbol{u}} \overset{\text{def}}{=} \tilde{\boldsymbol{u}}_1|_{\overline{\Omega}_1} + \tilde{\boldsymbol{u}}_2|_{\overline{\Omega}_2} + \cdots + \tilde{\boldsymbol{u}}_S|_{\overline{\Omega}_S}. \end{array}} \tag{24}$$

Table 1
The first four (unnormalized and normalized) statistical moments taken about the average

QN	$M_1^{Q_i-\Theta}$	$M_2^{Q_i-\Theta}$	$M_3^{Q_i-\Theta}$	$M_4^{Q_i-\Theta}$	$m_1^{Q_i-\Theta}$	$m_2^{Q_i-\Theta}$	$m_3^{Q_i-\Theta}$	$m_4^{Q_i-\Theta}$
κ^*	82.9187	0.1482	0.1094×10^{-02}	0.1354×10^{-02}	0	1	0.3356	2.8019
μ^*	29.4618	0.3595	0.1651×10^{-01}	0.4541×10^{-01}	0	1	0.3552	2.7164

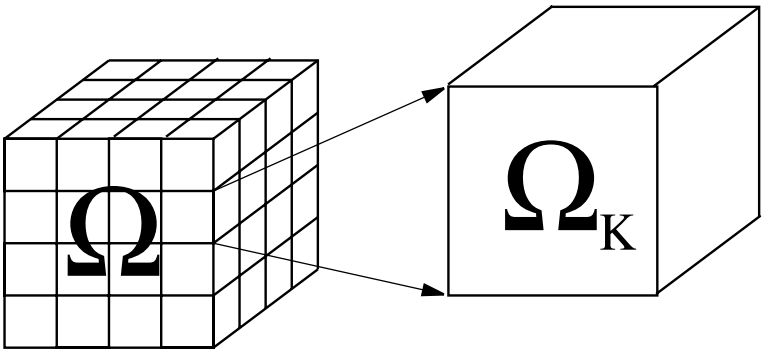

Fig. 9. The idea of partitioning a sample into smaller samples or equivalently combining smaller samples into a larger sample.

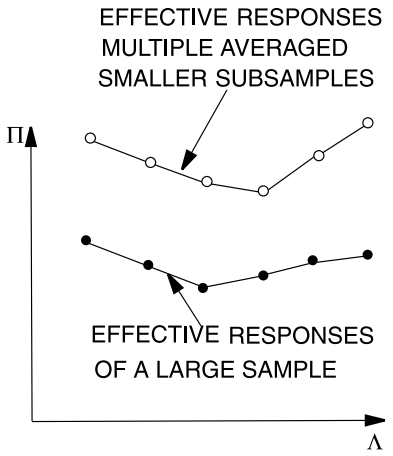

Fig. 10. Interpretation of the multiple subsample averaging technique.

The same process can be done for the traction test loading case: $\boldsymbol{t}|_{\partial\Omega_K} = \mathscr{L}\cdot\boldsymbol{n}$. The effective material ordering, line 3 in Box 24, has been derived by Huet [5]. The second line of Box 24, and generalizations to nonuniform loading, were developed in [35,38]. One can directly interpret the testing of many smaller samples as simply the partitioning of a large sample which cannot be easily test (Figs. 9 and 10). Therefore, for displacement tests, the averaged effective responses generated will always bound the response of the large sample, composed of the smaller samples, from above. Thus, minimization of the average of the responses of finite samples of material is equivalent to minimizing an upper bound on the effective property of a very large (still finite) statistically representative samples of material (Fig. 9). The proofs, which result from a direct manipulation of classical energy minimization principles, are provided next.

4.4. Decomposition of a sample of material

Consider a large sample whose domain consists of the union of many smaller subdomains, $\overline{\bigcup_{K=1}^{S}\Omega_K} = \overline{\Omega}$, as depicted in Fig. 9. The corresponding solution $\boldsymbol{u}$, denoted the globally exact solution, is characterized by the following variational boundary value problem:

$$\begin{aligned}&\text{Find } \boldsymbol{u}\in\boldsymbol{H}^1(\Omega),\ \boldsymbol{u}|_{\Gamma_u}=\boldsymbol{d},\ \text{such that}\\ &\underbrace{\int_\Omega \nabla\boldsymbol{v}:\boldsymbol{\sigma}\,\mathrm{d}\Omega}_{\stackrel{\text{def}}{=}\mathscr{B}(\boldsymbol{u},\boldsymbol{v})} = \underbrace{\int_\Omega \boldsymbol{f}\cdot\boldsymbol{v}\,\mathrm{d}\Omega+\int_{\Gamma_t}\boldsymbol{t}\cdot\boldsymbol{v}\,\mathrm{d}A}_{\stackrel{\text{def}}{=}\mathscr{F}(\boldsymbol{v})}\quad \forall\boldsymbol{v}\in\boldsymbol{H}^1(\Omega),\ \boldsymbol{v}|_{\Gamma_u}=\boldsymbol{0}.\end{aligned}\tag{25}$$

Specific choices for $\boldsymbol{d}$, $\boldsymbol{t}$ and $\boldsymbol{f}$ will be given momentarily. Now consider the boundary of an individual subdomain Ω_K, as $\partial\Omega_K$, $1 \leqslant K \leqslant S$ (S is the total number of subdomains)

$$\boxed{\begin{array}{l}\text{Find } \tilde{\boldsymbol{u}}_K \in \boldsymbol{H}^1(\Omega_K),\ \ \tilde{\boldsymbol{u}}_K|_{\partial\Omega_K \cap (\Omega \cup \Gamma_u)} = \boldsymbol{U} \in \boldsymbol{H}^1(\Omega), \quad \text{such that} \\ \quad \int_{\Omega_K} \nabla \boldsymbol{v}_K : \tilde{\boldsymbol{\sigma}}_K \, \mathrm{d}\Omega = \int_{\Omega_K} \boldsymbol{f} \cdot \boldsymbol{v}_K \, \mathrm{d}\Omega + \int_{\partial\Omega_K \cap \Gamma_t} \boldsymbol{t} \cdot \boldsymbol{v}_K \, \mathrm{d}A \\ \quad \forall \boldsymbol{v}_K \in \boldsymbol{H}^1(\Omega_K),\ \ \boldsymbol{v}_K|_{\partial\Omega_K \cap (\Omega \cup \Gamma_u)} = \boldsymbol{0}.\end{array}} \tag{26}$$

A specific choice for $\boldsymbol{U}$ will also be given momentarily. The individual subdomain solutions form an approximate solution to the globally exact problem, $\boldsymbol{u}$. This approximate solution is constructed by a direct assembly process

$$\boxed{\tilde{\boldsymbol{u}} \stackrel{\text{def}}{=} \boldsymbol{U} + (\tilde{\boldsymbol{u}}_1 - \boldsymbol{U})|_{\Omega_1} + (\tilde{\boldsymbol{u}}_2 - \boldsymbol{U})|_{\Omega_2} + \cdots + (\tilde{\boldsymbol{u}}_N - \boldsymbol{U})|_{\Omega_N}.} \tag{27}$$

The approximate displacement field is continuous, however, the approximate traction field is usually discontinuous. Clearly, if there are no jumps in the tractions, the solution is exact. For any kinematically admissible function $\boldsymbol{w}$, using the (bilinear operator) notation in Eq. (21), one has a definition of the so-called energy norm

$$0 \leqslant \|\boldsymbol{u} - \boldsymbol{w}\|^2_{E(\Omega)} \stackrel{\text{def}}{=} \mathscr{B}(\boldsymbol{u} - \boldsymbol{w}, \boldsymbol{u} - \boldsymbol{w}) = 2\mathscr{J}(\boldsymbol{w}) - 2\mathscr{J}(\boldsymbol{u}) \quad \Rightarrow \quad \mathscr{J}(\boldsymbol{u}) \leqslant \mathscr{J}(\boldsymbol{w}), \tag{28}$$

where we define the "elastic potential" by $\mathscr{J}(\boldsymbol{w}) \stackrel{\text{def}}{=} \frac{1}{2}\mathscr{B}(\boldsymbol{w}, \boldsymbol{w}) - \mathscr{F}(\boldsymbol{w})$. The potential relation in Eq. (28) is a form of the principle of minimum potential energy (PMPE). By applying the PMPE, for the test loading $\boldsymbol{u}|_{\partial\Omega} = \mathscr{E} \cdot \boldsymbol{x} = \boldsymbol{d}$, $\boldsymbol{f} = \boldsymbol{0}$, with the specific (kinematically admissible) choice $\boldsymbol{w} = \boldsymbol{U}$, one obtains

$$\|\boldsymbol{u} - \boldsymbol{U}\|^2_{E(\Omega)} = 2(\mathscr{J}(\boldsymbol{U}) - \mathscr{J}(\boldsymbol{u})) \quad \Rightarrow \quad \mathscr{J}(\boldsymbol{u}) = \mathscr{J}(\boldsymbol{U}) - \frac{1}{2}\|\boldsymbol{u} - \boldsymbol{U}\|^2_{E(\Omega)}. \tag{29}$$

The critical observation is that when choosing $\boldsymbol{w} = \boldsymbol{U} \stackrel{\text{def}}{=} \mathscr{E} \cdot \boldsymbol{x}$ in Box 26, then $\tilde{\boldsymbol{u}}$, as defined in Box 27, is also kinematically admissible. Therefore, by direct expansion

$$\|\boldsymbol{u} - \tilde{\boldsymbol{u}}\|^2_{E(\Omega)} = 2(\mathscr{J}(\tilde{\boldsymbol{u}}) - \mathscr{J}(\boldsymbol{u})) = 2(\mathscr{J}(\tilde{\boldsymbol{u}}) - \mathscr{J}(\boldsymbol{U})) + \|\boldsymbol{u} - \boldsymbol{U}\|^2_{E(\Omega)}. \tag{30}$$

Since $\tilde{\boldsymbol{u}}_K$ is a solution to a subdomain boundary value problem posed over Ω_K, it minimizes the corresponding subdomain potential energy function $\mathscr{J}_K(\cdot)$. Therefore

$$\mathscr{J}(\boldsymbol{U}) = \sum_{K=1}^{S} \mathscr{J}_K(\boldsymbol{U}) \geqslant \sum_{K=1}^{S} \mathscr{J}_K(\tilde{\boldsymbol{u}}_K) = \mathscr{J}(\tilde{\boldsymbol{u}}). \tag{31}$$

Consequently, $\|\boldsymbol{u} - \tilde{\boldsymbol{u}}\|^2_{E(\Omega)} = 2(\mathscr{J}(\tilde{\boldsymbol{u}}) - \mathscr{J}(\boldsymbol{U})) + \|\boldsymbol{u} - \boldsymbol{U}\|^2_{E(\Omega)}$, and by direct expansion one has $\|\boldsymbol{u} - \boldsymbol{U}\|^2_{E(\Omega)} = \mathscr{E} : (\langle \mathbb{E} \rangle - \mathbb{E}^*) : \mathscr{E}|\Omega| \leqslant \mathscr{E} : (\langle \mathbb{E} \rangle - \langle \mathbb{E}^{-1} \rangle^{-1}) : \mathscr{E}|\Omega|$. It follows that $2\mathscr{J}(\boldsymbol{U}) = \mathscr{E} : \langle \mathbb{E} \rangle : \mathscr{E}|\Omega|$, $2\mathscr{J}(\boldsymbol{u}) = \mathscr{E} : \mathbb{E}^* : \mathscr{E}|\Omega|$ and $2\mathscr{J}_K(\tilde{\boldsymbol{u}}) = \mathscr{E} : \tilde{\boldsymbol{E}}^*_K : \mathscr{E}|\Omega_K| \ \Rightarrow \ 2\mathscr{J}(\tilde{\boldsymbol{u}}) = \mathscr{E} : \tilde{\boldsymbol{E}}^* : \mathscr{E}|\Omega|$, which when substituted into Equation 31, yields the results in Box 24. Related results are discussed in [5,35,38].

5. Numerical simulations

In the numerical experiments, a quasi-Newton Level III method was used, within the following algorithm:

Step 1:	Statistically compute internal fields: $\boldsymbol{\Lambda} \pm h_{\Lambda_i}$ (until stabilized)
Step 2:	Post process results to obtain $\frac{\partial \Pi(\Lambda)}{\partial \Lambda_i}$, $\frac{\partial^2 \Pi(\Lambda)}{\partial \Lambda_i \partial \Lambda_j}$, $i, j = 1, \ldots, N$
Step 3:	Solve quasi-Newton Hessian system $\Rightarrow \Delta\boldsymbol{\Lambda}$
Step 4:	Update $\Lambda_i^{\text{new}} = \Lambda_i^{\text{old}} + \Delta\Lambda_i$, $i = 1, \ldots, N$
Step 5:	Go to Step 1 and repeat until: $\|\Pi\| \leqslant \text{TOL}$

It is remarked that for both manufacturing and physical reasons, each design variable must have a constrained search space. For example none of the design variables in this work can be negative, the volume fractions must be less than one, etc. One can employ penalty or barrier augmentations to constrain searches. However, in the numerical experiments, none of these approaches were needed, since the design search always located a local minimum within the feasible region. However, for the sake of completeness, constrained searches are discussed briefly in Appendix B.

During the optimization tests, successively larger samples of material were considered. It was found that samples containing approximately 20 particles with a 5% perturbation level ($h_i = \Lambda_i \times 0.05$) for the derivative increments, delivered stable results. In other words, larger samples and/or smaller derivative step sizes, produced negligibly different results. A fixed mesh of approximately $9 \times 9 \times 9$ trilinear hexahedra or 2778 numerical degrees of freedom *per particle*, for a total 46,875 degrees of freedom, was used. This mesh density delivered mesh independent results over the course of the numerical experiments. In other words, the same final designs occured using finer meshes. To illustrate the search process, continuing with 20 particle samples, the effective response produced by a sample containing approximately 22% boron spheres in an aluminum matrix ($\zeta = 0.75$) was first computed. The effective response was approximately

Table 2
Design iterations for various starting design vectors (EV = objective function evaluations)

Λ	I	EV	Π	κ^*	μ^*	κ_2/κ_1	μ_2/μ_1	ζ	AR	s
Λ_1	0	5	43.0355	121.9383	66.9111	5.0000	9.0000	0.7500	1.0000	4.0000
Λ_1	1	60	14.6804	110.2290	56.5813	4.8959	8.9404	0.6970	0.9861	3.9390
Λ_1	2	129	0.5956	97.9156	44.9920	4.9482	9.3864	0.6413	0.9819	2.9463
Λ_1	3	266	0.0551	97.2200	42.7849	5.0090	7.1986	0.6172	0.9844	3.6799
Λ_2	0	5	68.6828	128.6778	73.4867	5.0000	9.0000	0.7500	1.0000	6.0000
Λ_2	1	57	25.2377	114.9059	61.2453	4.9252	8.6266	0.6978	0.9881	5.8058
Λ_2	2	126	3.6597	102.6652	49.6137	5.1507	9.4512	0.6227	0.9867	5.6769
Λ_2	3	235	0.2370	96.9379	44.1224	5.0483	9.1170	0.5846	0.9861	5.5350
Λ_2	4	399	0.0589	94.7367	41.1414	4.9934	8.9511	0.5688	0.9816	5.4335
Λ_3	0	5	81.5071	131.6331	76.3758	5.0000	9.0000	0.7500	1.0000	8.0000
Λ_3	1	54	26.6939	115.0966	62.0680	4.8872	8.6936	0.6896	0.9926	8.0119
Λ_3	2	112	9.0704	107.5425	53.5791	4.8273	8.3963	0.6534	0.9773	8.0812
Λ_3	3	206	0.2205	99.6734	43.2056	4.6661	5.4589	0.6122	0.9892	8.1625
Λ_3	4	330	0.1083	98.4434	42.8631	4.9781	6.2456	0.5965	0.9876	8.0551
Λ_4	0	5	88.9532	133.2589	77.9655	5.0000	9.0000	0.7500	1.0000	10.0000
Λ_4	1	51	27.9507	116.0929	62.3040	4.8862	8.6912	0.6872	0.9924	10.0256
Λ_4	2	123	23.6082	111.7716	61.8776	5.6605	10.8395	0.6445	0.9857	11.4297
Λ_4	3	200	4.5931	101.5765	50.3933	7.6708	11.5097	0.5704	0.9847	11.6022
Λ_4	4	277	0.1342	93.9655	40.7742	7.9004	8.1025	0.5245	0.9831	11.1578
Λ_5	0	5	99.9732	135.5157	80.0877	5.0000	9.0000	0.7500	1.0000	20.0000
Λ_5	1	51	32.6924	117.5604	64.0404	4.9050	8.7880	0.6862	0.9922	20.0867
Λ_5	2	127	7.9106	106.1167	53.4303	4.6413	8.2295	0.6326	0.9847	19.8505
Λ_5	3	233	0.2154	93.6492	40.3829	4.7319	8.5882	0.5360	0.9868	20.0609
Λ_5	4	356	0.1369	94.7746	40.5122	4.6691	7.2650	0.5504	0.9977	20.2028
Λ_6	0	5	62.2174	126.5115	72.0773	6.0000	10.0000	0.7500	1.0000	4.0000
Λ_6	1	54	29.6293	116.1527	62.7850	5.8391	9.9684	0.7112	0.9894	3.9259
Λ_6	2	118	2.0628	102.1446	47.3256	5.8376	8.5113	0.6632	0.9843	3.0651
Λ_6	3	221	0.0887	97.4128	43.0547	5.7384	8.2854	0.6287	0.9743	2.9849
Λ_7	0	5	141.8073	142.2823	87.4796	6.0000	10.0000	0.7500	1.0000	20.0000
Λ_7	1	54	51.1333	121.5352	69.9154	5.8950	9.7981	0.6877	0.9915	20.0906
Λ_7	2	122	13.0550	109.3701	55.9280	5.7013	8.7954	0.6364	0.9876	20.2199
Λ_7	3	210	6.6772	104.3111	52.3190	13.6811	8.6646	0.5717	0.9942	19.9531
Λ_7	4	293	0.1744	93.4774	40.6840	13.1676	8.9672	0.4946	0.9956	19.8462

The iterations were terminated when $\Pi \leqslant 0.2$.

$\kappa^* = 96$ GPa and $\mu^* = 42$ GPa. Our objective was to find alternative microstructures which could deliver the same effective response, to a specified tolerance. With this in mind, the algorithm was started away from the original spherical aluminum/boron design space location, however, still prescribing the same objective: $\kappa^{*\mathrm{D}} = 96$ GPa and $\mu^{*\mathrm{D}} = 42$ GPa. The matrix material was fixed to be aluminum, however, all other design parameters were allowed to vary. Microstructures of very stiff particles, of successively more "blocklike" structure: exponent $s = 4$, 6, 8, 10, and 20, were starting design vectors, and allowed the algorithm to "carve down" to an appropriate shape, volume fraction and a set of mechanical stiffnesses to meet a target

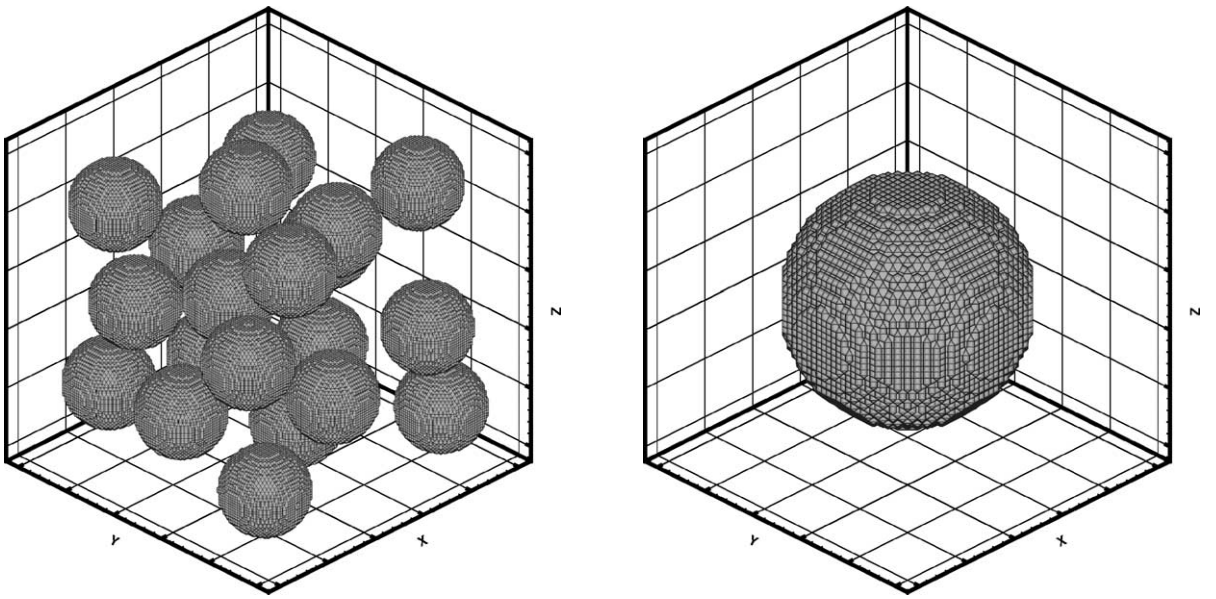

Fig. 11. The original spherical microstructure: $(\kappa_2/\kappa_1) = 2.9525$, $(\mu_2/\mu_1) = 6.9076$, $\zeta = 0.75$ (volume fraction: $v_2 \approx 0.2209$), AR $= 1.00$, $s = 2.00$.

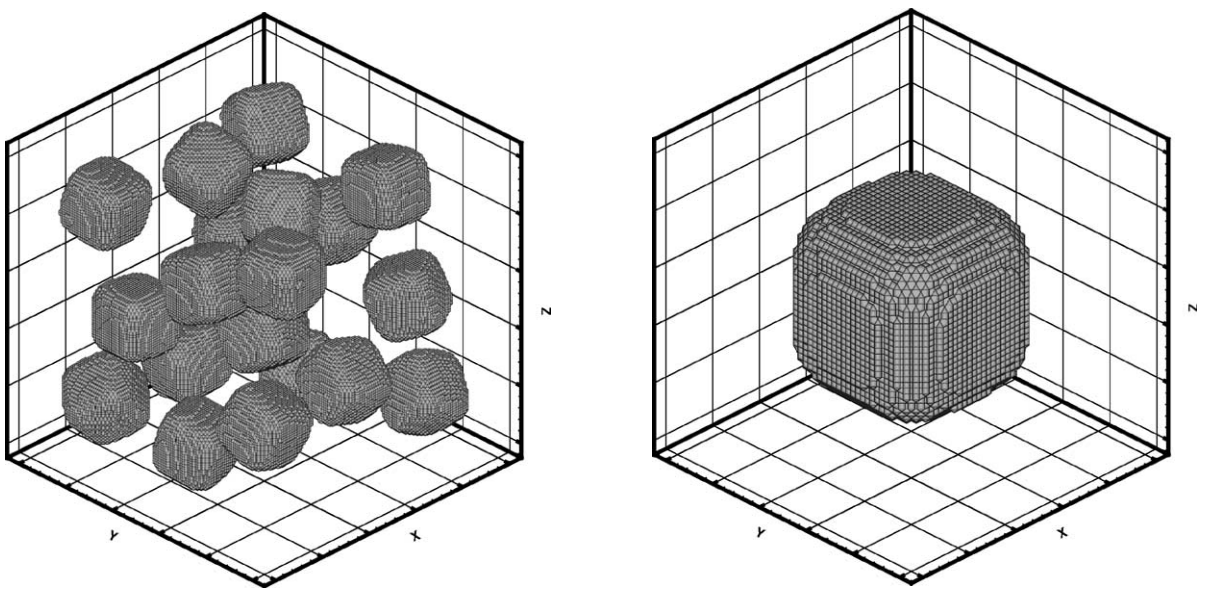

Fig. 12. Optimum found from starting at Λ_1: $(\kappa_2/\kappa_1) = 5.0090$, $(\mu_2/\mu_1) = 7.1986$, $\zeta = 0.6172$ (volume fraction: $v_2 \approx 0.1896$), AR $= 0.9844$, $s = 3.6799$.

tolerable value of the objective function. In all of the simulations to follow the the macroscopic bulk and shear weights were $w_\kappa = w_\mu = 100$, and $q_\kappa = q_\mu = 2$. The adaptive multiple sampling average tolerance (Eq. (23)) was set to $\mathrm{TOL}_A = 0.01$. The starting design vectors, and the final design vectors, are those shown in Table 2. The corresponding topologies of various designs generated are shown in Figs. 11–18. From a practical point of view, the results serve as guides for alternative particulate additive material, volume fraction and topology selection to boron spheres.

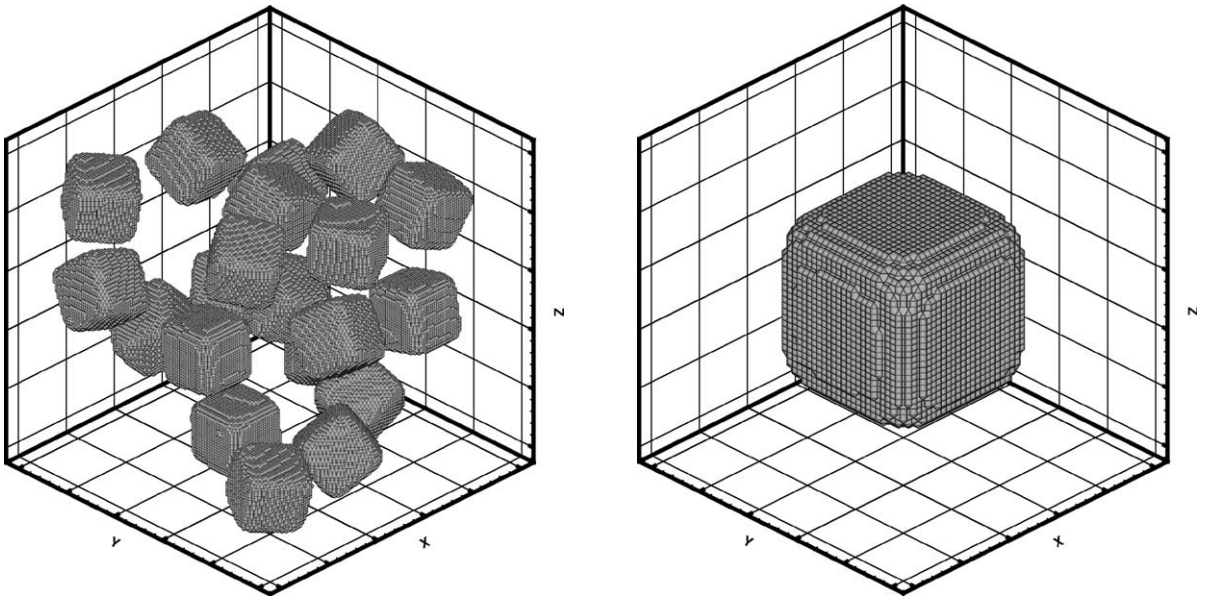

Fig. 13. Optimum found from starting at Λ_2: $(\kappa_2/\kappa_1) = 4.9934$, $(\mu_2/\mu_1) = 8.9511$, $\zeta = 0.5688$ (volume fraction: $v_2 \approx 0.1705$), AR $= 0.9816$, $s = 5.4335$.

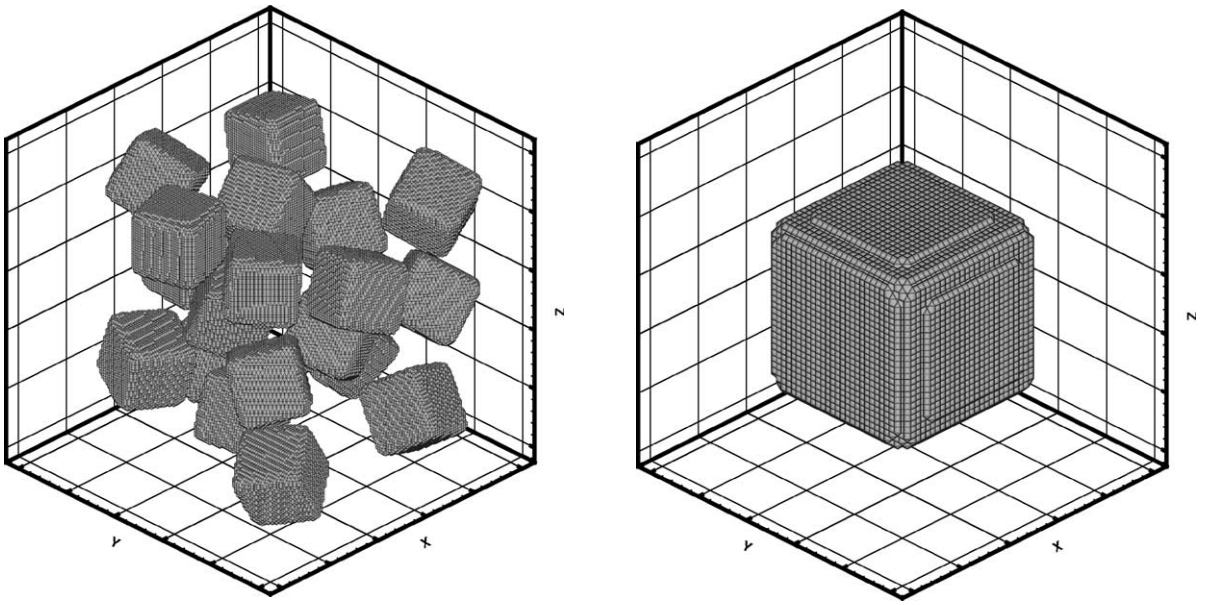

Fig. 14. Optimum found from starting at Λ_3: $(\kappa_2/\kappa_1) = 4.9781$, $(\mu_2/\mu_1) = 6.2456$, $\zeta = 0.5956$ (volume fraction: $v_2 \approx 0.2065$), AR $= 0.9876$, $s = 8.0551$.

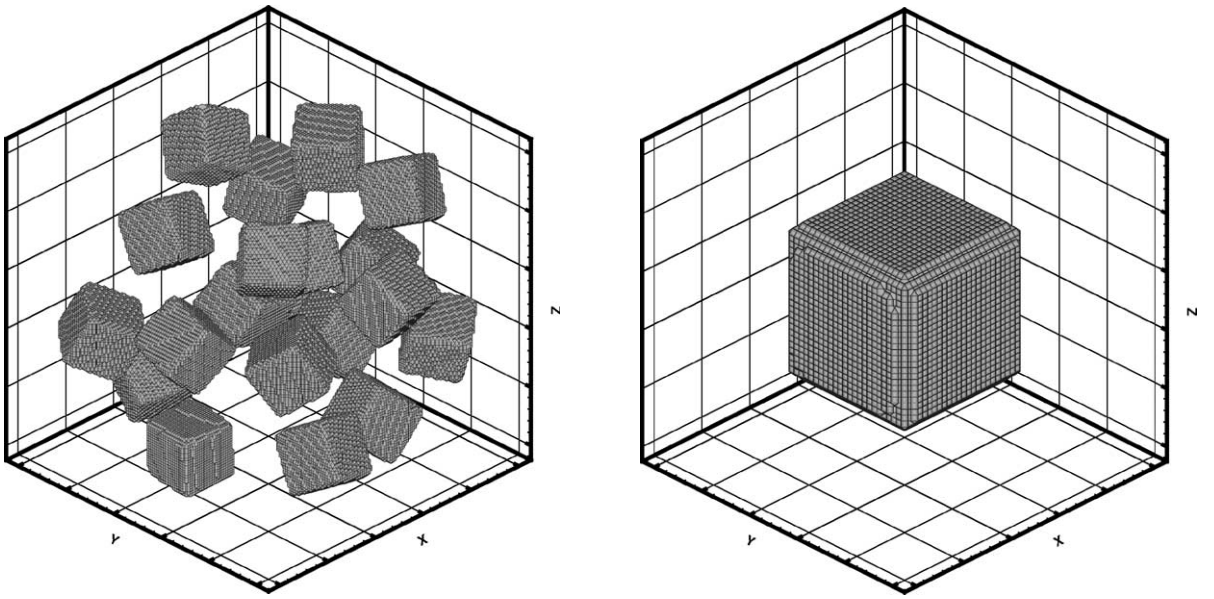

Fig. 15. Optimum found from starting at Λ_4: $(\kappa_2/\kappa_1) = 7.9004$, $(\mu_2/\mu_1) = 8.1025$, $\zeta = 0.5245$ (volume fraction: $v_2 \approx 0.1500$), AR $= 0.9831$, $s = 11.1578$.

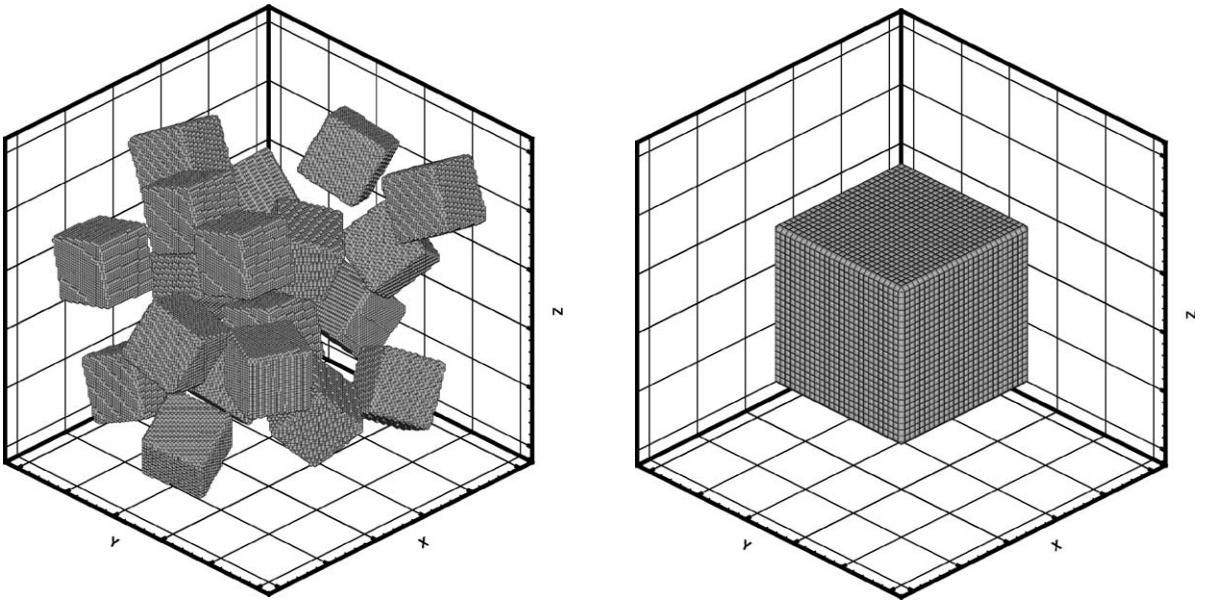

Fig. 16. Optimum found from starting at Λ_5: $(\kappa_2/\kappa_1) = 4.6691$, $(\mu_2/\mu_1) = 7.2650$, $\zeta = 0.5504$ (volume fraction: $v_2 \approx 0.1581$), AR $= 0.9977$, $s = 20.2028$.

6. Concluding remarks

As shown in the numerical experiments there are multiple local minima. To determine the variety of design possibilities, one must start searches from several starting locations to seek out various local optima. This can be quite computationally intensive, however, there are *two* levels of parallelism possible. The first level of parallelism is that the derivatives needed in quasi-Newton (Level III) processes can be computed independently, since the terms in the Hessian have no interaction between one another during the assembly

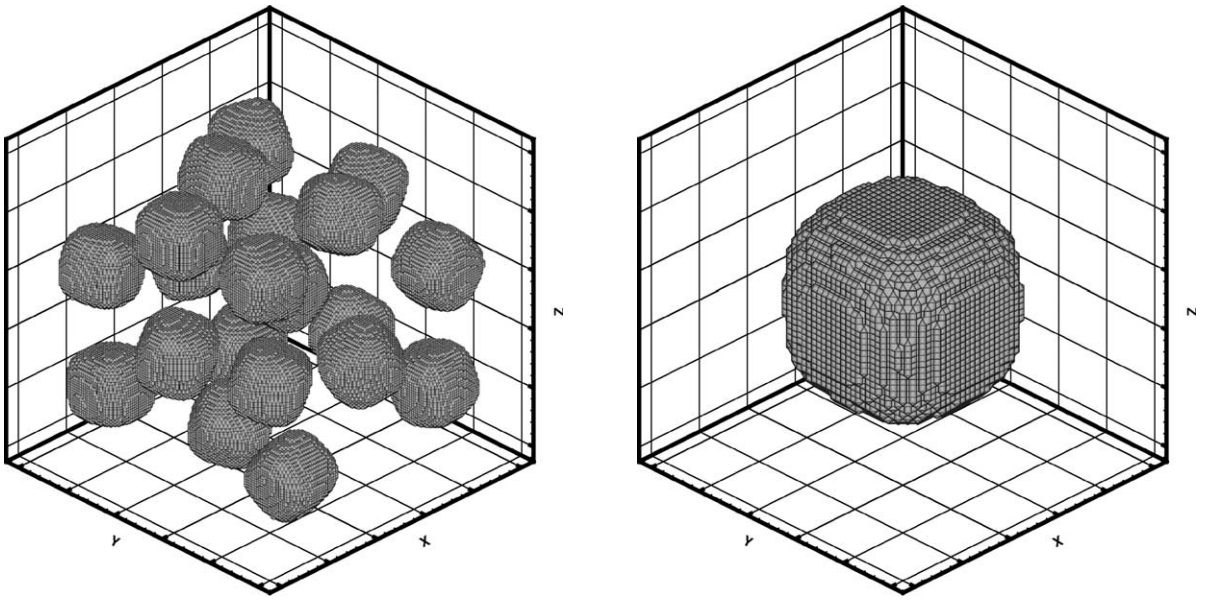

Fig. 17. Optimum found from starting at Λ_6: $(\kappa_2/\kappa_1) = 5.7384$, $(\mu_2/\mu_1) = 8.2854$, $\zeta = 0.6287$ (volume fraction: $v_2 \approx 0.1781$), AR $= 0.9743$, $s = 2.9849$.

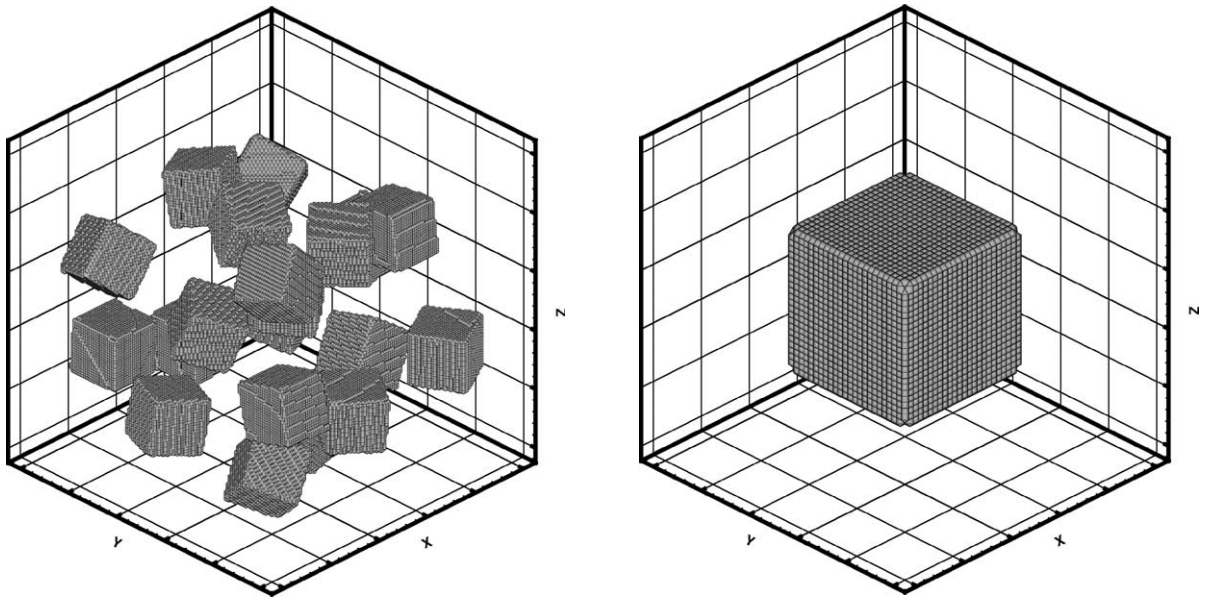

Fig. 18. Optimum found from starting at Λ_7: $(\kappa_2/\kappa_1) = 13.1676$, $(\mu_2/\mu_1) = 8.9672$, $\zeta = 0.4946$ (volume fraction: $v_2 \approx 0.1255$), AR $= 0.9956$, $s = 19.8462$.

process. The second level of parallelism is that the multiple searches themselves can be performed independently from one another. An alternative approach to multiple search quasi-Newton methods are the so-called global optimization (GO) techniques based upon rapid, stochastic function evaluation. Loosely speaking, they are methods of "popping out" of local convex minimum wells, and thus provides a possible way to find a global minimum, if it exists. For reviews of such methods, the interested reader is referred to [32] for information on genetic algorithms, and [37,36] for theories of global random search. The possible use of such algorithms is under investigation by the author.

Appendix A. A closeup of BFGS

The key feature of the Newton method that makes it so effective in optimization is that it contains off-diagonal second-order derivative information on the interaction of the design variables. Level I and Level II approaches contain no such information. Quasi-Newton methods start at Level I or II for the first iteration then successively update the Hessian matrix with gradient information from the previous iterations. For example, one could keep storing values of the gradient, $\{\boldsymbol{g}^{(1)}\}, \{\boldsymbol{g}^{(2)}\}, \ldots, \{\boldsymbol{g}^{(k)}\}$ and construct approximate Hessians via [2]

$$H_{ij}^{(k)} = \frac{\partial}{\partial D_i^{(k)}}\left(\frac{\partial \Pi^{(k)}}{\partial D_j^{(k)}}\right) = \frac{\partial g_j^{(k)}}{\partial D_i^{(k)}} = \frac{1}{D_i^{(k+1)} - D_i^{(k)}}\left(g_j^{(k+1)} - g_j^{(k)}\right). \tag{32}$$

Thereafter, to induce symmetry, the following is performed, $[\mathbb{H}^{(k)}] = \frac{1}{2}([\mathbb{H}^{(k)}] + [\mathbb{H}^{(k,\mathrm{T})}])$. A clever and efficient way of constructing approximate Hessians is the essence of the quasi-Newton family. This is an extremely well-studied topic dating back, at least to the seminal work of Davidon [29] and subsequent improvements by Fletcher and Powell [30]. An exhaustive review of these methods can be found in the classical texts of Luenberger [34] or Gill et al. [33]. Only the basic points are summarized next.

A.1. Construction of updates

Define the following: (1) $\{\Delta\boldsymbol{\Lambda}^{(k)}\} = \{\boldsymbol{\Lambda}^{(k+1)}\} - \{\boldsymbol{\Lambda}^{(k)}\}$, (2) $\{\Delta\boldsymbol{g}^{(k)}\} = \{\boldsymbol{g}^{(k+1)}\} - \{\boldsymbol{g}^{(k)}\}$, (3) $[\boldsymbol{A}^{(k)}]$ is an updated approximation to $[\mathbb{H}^{(k)}]$ and (4) $[\boldsymbol{A}^{(0)}] = [\boldsymbol{I}]$. One seeks to find an update $[\boldsymbol{U}^{(k)}]$ where $[\boldsymbol{A}^{(k+1)}] = [\boldsymbol{A}^{(k)}] + [\boldsymbol{U}^{(k)}]$.

A.2. Rank-one updates

Let us expand the gradient about $\{\boldsymbol{\Lambda}^{(k)}\}$ in a Taylor series, $\{\boldsymbol{g}^{(k+1)}\} = \{\boldsymbol{g}^{(k)}\} + [\mathbb{H}^{(k)}]\{\Delta\boldsymbol{\Lambda}^{(k)}\}$. The curvature of Π along $\Delta\{\boldsymbol{\Lambda}^{(k)}\}$ is $\{\Delta\boldsymbol{\Lambda}^{(k)}\}^{\mathrm{T}}[\mathbb{H}^{(k)}]\{\Delta\boldsymbol{\Lambda}^{(k)}\} \approx \{\Delta\boldsymbol{\Lambda}^{(k)}\}^{\mathrm{T}}\{\Delta\boldsymbol{g}^{(k)}\}$, which is of course exact for a quadratic function. Therefore the standard condition for the approximate Hessian is that it should approximate the curvature of Π along $\{\Delta\boldsymbol{\Lambda}^{(k)}\}$. Thus, $\{\Delta\boldsymbol{\Lambda}^{(k)}\}^{\mathrm{T}}[\boldsymbol{A}^{(k+1)}]\{\Delta\boldsymbol{\Lambda}^{(k)}\} = \{\Delta\boldsymbol{\Lambda}^{(k)}\}^{\mathrm{T}}(\{\boldsymbol{g}^{(k+1)}\} - \{\boldsymbol{g}^{(k)}\}) = \{\Delta\boldsymbol{g}^{(k)}\}\{\Delta\boldsymbol{\Lambda}^{(k)}\}$, which implies $[\boldsymbol{A}^{(k+1)}]\{\Delta\boldsymbol{\Lambda}^{(k)}\} = \{\Delta\boldsymbol{g}^{(k)}\}$. During a single iteration the new information about the second-order behavior of Π is only in one direction. Therefore one would expect $[\boldsymbol{A}^{(k+1)}] - [\boldsymbol{A}^{(k)}]$ to be a low rank matrix of the form $[\boldsymbol{A}^{(k+1)}] = [\boldsymbol{A}^{(k)}] + \{\boldsymbol{l}^{(k)}\}\{\boldsymbol{r}^{(k)}\}^{\mathrm{T}}$, where $\{\boldsymbol{l}^{(k)}\}$ and $\{\boldsymbol{r}^{(k)}\}$ are vectors. A matrix of the form $\{\boldsymbol{l}^{(k)}\}\{\boldsymbol{r}^{(k)}\}^{\mathrm{T}}$ is termed rank-one. The quasi-Newton condition is then $[\boldsymbol{A}^{(k+1)}]\{\Delta\boldsymbol{\Lambda}^{(k)}\} = ([\boldsymbol{A}^{(k)}] + \{\boldsymbol{l}^{(k)}\}\{\boldsymbol{r}^{(k)}\}^{\mathrm{T}})\{\Delta\boldsymbol{\Lambda}^{(k)}\} = \{\Delta\boldsymbol{g}^{(k)}\}$, and implies $\{\boldsymbol{l}^{(k)}\}(\{\boldsymbol{r}^{(k)}\}^{\mathrm{T}}\{\Delta\boldsymbol{\Lambda}^{(k)}\}) = \{\Delta\boldsymbol{g}^{(k)}\} - [\boldsymbol{A}^{(k)}]\{\Delta\boldsymbol{\Lambda}^{(k)}\}$. Therefore $\{\boldsymbol{l}^{(k)}\}$ must be in the same direction as $\{\Delta\boldsymbol{g}^{(k)}\} - [\boldsymbol{A}^{(k)}]\{\Delta\boldsymbol{\Lambda}^{(k)}\}$, since $\{\boldsymbol{r}^{(k)}\}\{\Delta\boldsymbol{\Lambda}^{(k)}\}$ is a scalar. For any vector $\{\boldsymbol{r}^{(k)}\}$ such that $\{\boldsymbol{r}^{(k)}\}^{\mathrm{T}}\{\Delta\boldsymbol{\Lambda}^{(k)}\}$ is nonzero, the vector $\{\boldsymbol{l}^{(k)}\}$ is given by $\{\boldsymbol{l}^{(k)}\} = (1/\{\boldsymbol{r}^{(k)}\}^{\mathrm{T}}\{\Delta\boldsymbol{\Lambda}^{(k)}\})(\{\Delta\boldsymbol{g}^{(k)}\} - [\boldsymbol{A}^{(k)}]\{\Delta\boldsymbol{\Lambda}^{(k)}\})$. However, since the Hessian matrix must be symmetric, one seeks updates which preserve this property. The rank-one updates requirement of "symmetry of inheritance" uniquely determines the update. In order for the update to maintain symmetry of $[\boldsymbol{A}^{(k)}]$, $\{\boldsymbol{r}^{(k)}\}$ must be a multiple of $\{\boldsymbol{l}^{(k)}\}$, therefore,

$$\begin{aligned}[\boldsymbol{A}^{(k+1)}] = [\boldsymbol{A}^{(k+1,\mathrm{T})}] &= [\boldsymbol{A}^{(k)}]^{\mathrm{T}} + \frac{1}{\{\boldsymbol{r}^{(k)}\}^{\mathrm{T}}\{\Delta\boldsymbol{\Lambda}^{(k)}\}}\{\boldsymbol{r}^{(k)}\}\left(\{\Delta\boldsymbol{g}^{(k)}\} - [\boldsymbol{A}^{(k)}]\{\Delta\boldsymbol{\Lambda}^{(k)}\}\right)^{\mathrm{T}} \\ &= [\boldsymbol{A}^{(k)}] + \frac{1}{\{\boldsymbol{r}^{(k)}\}^{\mathrm{T}}\{\Delta\boldsymbol{\Lambda}^{(k)}\}}\left(\{\Delta\boldsymbol{g}^{(k)}\} - [\boldsymbol{A}^{(k)}]\{\Delta\boldsymbol{\Lambda}^{(k)}\}\right)\{\boldsymbol{r}^{(k)}\}^{\mathrm{T}},\end{aligned} \tag{33}$$

which implies $\{\boldsymbol{r}^{(k)}\} = (\{\Delta\boldsymbol{g}^{(k)}\} - [\boldsymbol{A}^{(k)}]\{\Delta\boldsymbol{\Lambda}^{(k)}\})$. This is the only choice for a symmetric rank-one update.

[2] T = transpose.

A.3. Rank-two updates

In general if one has $[\boldsymbol{A}^{(1)}] = [\boldsymbol{A}^{(0)}] + \{\boldsymbol{l}^{(k)}\}\{\boldsymbol{r}^{(k)}\}^{\mathrm{T}}$, this satisfies the quasi-Newton condition $[\boldsymbol{A}^{(1)}]\{\Delta\boldsymbol{\Lambda}^{(0)}\} = \{\Delta\boldsymbol{g}^{(0)}\}$, which implies $([\boldsymbol{A}^{(0)}] + \{\boldsymbol{l}^{(k)}\}\{\boldsymbol{r}^{(k)}\})\{\Delta\boldsymbol{\Lambda}^{(0)}\}^{\mathrm{T}} = \{\Delta\boldsymbol{g}^{(0)}\}$, and consequently $(\{\boldsymbol{l}^{(k)}\}\{\boldsymbol{r}^{(k)}\}^{\mathrm{T}})\{\Delta\boldsymbol{\Lambda}^{(0)}\} = \{\Delta\boldsymbol{g}^{(0)}\} - [\boldsymbol{A}^{(0)}]\{\Delta\boldsymbol{\Lambda}^{(0)}\}$. However, $[\boldsymbol{A}^{(1)}]$ is not symmetric and therefore one defines $[\boldsymbol{A}^{(2)}] = \frac{1}{2}([\boldsymbol{A}^{(1)}] + [\boldsymbol{A}^{(1,\mathrm{T})}])$. However, $\boldsymbol{A}^{(2)}$ will not satisfy the quasi-Newton condition $[\boldsymbol{A}^{(2)}]\{\Delta\boldsymbol{\Lambda}^{(1)}\} \neq \{\Delta\boldsymbol{g}^{(1)}\}$, which implies $([\boldsymbol{A}^{(1)}] + \{\boldsymbol{l}^{(1)}\}\{\boldsymbol{r}^{(\mathrm{T})}\}^{\mathrm{T}})\{\Delta\boldsymbol{\Lambda}^{(1)}\} \neq \{\Delta\boldsymbol{g}^{(1)}\}$, and consequently implies $(\{\boldsymbol{l}^{(1)}\}\{\boldsymbol{r}^{(1)}\}^{\mathrm{T}})\{\Delta\boldsymbol{\Lambda}^{(1)}\} \neq \{\Delta\boldsymbol{g}^{(1)}\} - [\boldsymbol{A}^{(1)}]\{\Delta\boldsymbol{\Lambda}^{(1)}\}$. Therefore, one repeats the quasi-Newton update $[\boldsymbol{A}^{(3)}] = [\boldsymbol{A}^{(2)}] + (1/\{\boldsymbol{r}^{(k)}\}^{\mathrm{T}}\{\Delta\boldsymbol{\Lambda}^{(k)}\})(\{\Delta\boldsymbol{g}^{(k)}\} - [\boldsymbol{A}^{(2)}]\{\Delta\boldsymbol{\Lambda}^{(k)}\})\{\boldsymbol{r}^{(k)}\}^{\mathrm{T}}$, or in general $[\boldsymbol{A}^{(2j+1)}] = [\boldsymbol{A}^{(2j)}] + (1/\{\boldsymbol{r}^{(k)}\}\{\Delta\boldsymbol{\Lambda}^{(k)}\})(\{\Delta\boldsymbol{g}^{(k)}\} - [\boldsymbol{A}^{(2j)}]\{\Delta\boldsymbol{\Lambda}^{(k)}\})\{\boldsymbol{r}^{(k)}\}^{\mathrm{T}}$ and $[\boldsymbol{A}^{(2j+2)}] = \frac{1}{2}([\boldsymbol{A}^{(2j+1)}] + [\boldsymbol{A}^{(2j+1,\mathrm{T})}])$. Taking the limit as $j = 0, 1, \ldots$, one obtains

$$\boxed{\begin{aligned}[\boldsymbol{A}^{(k+1)}] = [\boldsymbol{A}^{(k)}] &+ \frac{1}{\{\boldsymbol{r}^{(k)}\}^{\mathrm{T}}\{\Delta\boldsymbol{\Lambda}^{(k)}\}}(\{\Delta\boldsymbol{g}^{(k)}\} - [\boldsymbol{A}^{(k)}]\{\Delta\boldsymbol{\Lambda}^{(k)}\}) + \{\boldsymbol{r}^{(k)}\}^{\mathrm{T}}(\{\Delta\boldsymbol{g}^{(k)}\} - [\boldsymbol{A}^{(k)}]\{\Delta\boldsymbol{\Lambda}^{(k)}\})^{\mathrm{T}} \\ &- \frac{1}{(\{\boldsymbol{r}^{(k)}\}^{\mathrm{T}}\{\Delta\boldsymbol{\Lambda}^{(k)}\})^2}(\{\Delta\boldsymbol{g}^{(k)}\} - [\boldsymbol{A}^{(k)}]\{\Delta\boldsymbol{\Lambda}^{(k)}\})^{\mathrm{T}}\{\Delta\boldsymbol{\Lambda}^{(k)}\})\{\boldsymbol{r}^{(k)}\}\{\boldsymbol{r}^{(k)}\}^{\mathrm{T}}.\end{aligned}} \tag{34}$$

Therefore, one has (1) when $\{\boldsymbol{r}^{(k)}\} = \{\Delta\boldsymbol{\Lambda}^{(k)}\}$ this is the well-known Powell-symmetric-Broyden (PsB) update and (2) when $\{\boldsymbol{r}^{(k)}\} = \{\Delta\boldsymbol{g}^{(k)}\}$ this is the well-known Davidson–Fletcher–Powell (DFP) update. This is a well-defined rank-two update for any $\{\boldsymbol{r}^{(k)}\}^{\mathrm{T}}$ that is not orthogonal to $\Delta\{\boldsymbol{\Lambda}^{(k)}\}$. The rank-two analog to the symmetric rank-one update can be derived by setting $(\{\Delta\boldsymbol{g}^{(k)}\} - [\boldsymbol{A}^{(k)}])$. One can expand the general expression to obtain

$$\boxed{\begin{aligned}[\boldsymbol{A}^{(k+1)}] = [\boldsymbol{A}^{(k)}] &+ \frac{1}{\{\Delta\boldsymbol{\Lambda}^{(k)}\}^{\mathrm{T}}[\boldsymbol{A}^{(k)}]\{\Delta\boldsymbol{\Lambda}^{(k)}\}}([\boldsymbol{A}^{(k)}]\{\Delta\boldsymbol{\Lambda}^{(k)}\})([\boldsymbol{A}^{(K)}]\{\Delta\boldsymbol{\Lambda}^{(k)}\})^{\mathrm{T}} \\ &+ \frac{1}{\{\Delta\boldsymbol{g}^{(k)}\}^{\mathrm{T}}\{\Delta\boldsymbol{\Lambda}^{(k)}\}}\{\Delta\boldsymbol{g}^{(k)}\}\{\Delta\boldsymbol{g}^{(k)}\}^{\mathrm{T}} + \underbrace{(\{\Delta\boldsymbol{\Lambda}^{(k)}\}^{\mathrm{T}}[\boldsymbol{A}^{(k)}]\{\Delta\boldsymbol{\Lambda}^{(k)}\})\{\boldsymbol{s}^{(k)}\}\{\boldsymbol{s}^{(k)}\}^{\mathrm{T}}}_{\Theta},\end{aligned}} \tag{35}$$

where $\{\boldsymbol{s}^{(k)}\} \stackrel{\mathrm{def}}{=} (1/\{\Delta\boldsymbol{g}^{(k)}\}^{\mathrm{T}}\{\Delta\boldsymbol{\Lambda}^{(k)}\})\{\Delta\boldsymbol{g}^{(k)}\} - (1/\{\Delta\boldsymbol{\Lambda}^{(k)}\}^{\mathrm{T}}[\boldsymbol{A}^{(k)}]\{\Delta\boldsymbol{\Lambda}^{(k)}\})[\boldsymbol{A}^{(k)}]\{\boldsymbol{\Lambda}^{(k)}\}$. When $\boldsymbol{\Theta} = \{\boldsymbol{0}\}$ this is the well-known BFGS update.

Appendix B. Constrained searches

Generally, each design variable has bilateral constraints, $\Lambda_{i-} \leqslant \Lambda_i \leqslant \Lambda_{i+}$. A classical way to enforce bilateral constraints is by constructing a function whose unconstrained minimum is the optimal solution, or related to it in some known way. Owing to the fact that the unconstrained minimum may, during the optimization process, fall outside of the feasible regions, an *exterior* penalty function method is incorporated to push the optimization algorithm's search into the feasible region. In an attempt to force the search to remain in the feasible region, *interior* penalty functions are constructed. This is accomplished by adding to the original function, a function with a positive singularity at the boundary of the feasible region, a so-called *barrier*. As an example, consider the following hypothetical augmented exterior (penalty)-interior (barrier) function

$$\Pi = \underbrace{\Pi}_{\text{raw objective}} + \underbrace{\sum_{i=1}^{K}\left(\widehat{p}_i\left|\frac{Q_i - Q_i^+}{Q_i^+}\right|^{q_i^{\mathrm{P}}} + \widehat{p}_i\left|\frac{Q_i - Q_i^-}{Q_i^-}\right|^{q_i^{\mathrm{P}}}\right)}_{\text{penalty term} \stackrel{\mathrm{def}}{=} \mathbb{P}} + \underbrace{\sum_{i=1}^{K}\left(\widehat{b}_i\left|\frac{Q_i - Q_i^+}{Q_i^+}\right|^{-q_i^{\mathrm{B}}} + \widehat{b}_i\left|\frac{Q_i - Q_i^-}{Q_i^-}\right|^{-q_i^{\mathrm{B}}}\right)}_{\text{barrier term} \stackrel{\mathrm{def}}{=} \mathbb{B}}, \tag{36}$$

the Q_i are the design variables, the Q_i^- are the lower limit values for design variables, the Q_i^+ are the upper limit values for design variables, w_i are weights, K is the number of design variables. The $\widehat{p_i} = 0$ and $\widehat{b_i} = b_i$ in the feasible region and $\widehat{p_i} = p_i$ and $\widehat{b_i} = 0$ outside of the feasible region. As before, the q's represent positive constants.

B.1. Properties: exterior/penalty functions

Let us define the following unconstrained function $\Pi^{\mathrm{P}}(\aleph_K, \boldsymbol{p}_k) \stackrel{\mathrm{def}}{=} \Pi(\aleph_K) + \boldsymbol{p}_K \mathbb{P}(\aleph_K)$, where (1) $\mathbb{P}(\aleph_K) \in C^0(\mathbb{R}^N)$, (2) $\mathbb{P}(\aleph_K) \geq 0$ and (3) $\mathbb{P}(\aleph_K) = 0$, if and only if $\aleph_K \in \Theta_f$, $\Theta_f \stackrel{\mathrm{def}}{=}$ the feasible region. We have the following properties, where $\aleph_K^*$ is the minimizer of Π^{P} for weight $\boldsymbol{p}_K$ and $\aleph^*$ is the true minimizer for the exact problem Π with the constraints:

$$\begin{array}{ll}
\text{(a)} & \Pi^{\mathrm{P}}(\aleph_K^*, \boldsymbol{p}_K) \leqslant \Pi^{\mathrm{P}}(\aleph_{K+1}^*, \boldsymbol{p}_{K+1}), \\
\text{(b)} & \mathbb{P}(\aleph_{K+1}^*) \leqslant \mathbb{P}(\aleph_K^*), \\
\text{(c)} & \Pi^{\mathrm{P}}(\aleph_K^*) \leqslant \Pi^{\mathrm{P}}(\aleph_{K+1}^*), \\
\text{(d)} & \Pi(\aleph_K^*) \leqslant \Pi^{\mathrm{P}}(\aleph_K^*, \boldsymbol{p}_K) \leqslant \Pi(\aleph^*), \\
\text{(e)} & \lim_{\boldsymbol{p}_K \to \infty} \Pi^{\mathrm{P}}(\aleph_K^*, \boldsymbol{p}_K) = \Pi(\aleph^*).
\end{array} \tag{37}$$

The proofs of these results, which are classical, are included in the appendix for completeness. The important point is that for increasing penalty weights, we are assured to converge to a feasible minimum. In general one uses a series of weights, and stops at finitely large, penalty values. There are a variety of minor variations to such approaches since their introduction in the late 1960's, but the essential idea has remained unchanged. For more details we refer the interested reader to reviews in [31,34].

B.2. Properties: interior/barrier functions

The dual to exterior/penalty formulations, so-called barrier formulations are now discussed. Let us define the following unconstrained function, $\Pi^{\mathrm{B}}(\aleph_K, \boldsymbol{b}_k) \stackrel{\mathrm{def}}{=} \Pi(\aleph_K) + \boldsymbol{b}_K \mathbb{B}(\aleph_K)$, where (1) $\mathbb{B}(\aleph_K) \in C^0(\Theta_f)$, (2) $\mathbb{B}(\aleph_K) \geqslant 0$ and (3) $\mathbb{B}(\aleph_K) \to \infty$, if $\aleph_K \to \partial\Theta_f$. We have the following properties, where $\aleph_K^*$ is the minimizer of Π^{B} with weight $\boldsymbol{b}_K$ and $\aleph^*$ is the true minimizer for the exact problem with constraints:

$$\begin{array}{ll}
\text{(a)} & \Pi^{\mathrm{B}}(\aleph_K^*, \boldsymbol{b}_K) \geqslant \Pi^{\mathrm{B}}(\aleph_{K+1}^*, \boldsymbol{b}_{K+1}), \\
\text{(b)} & \mathbb{B}(\aleph_{K+1}^*) \geqslant \mathbb{B}(\aleph_K^*), \\
\text{(c)} & \Pi^{\mathrm{B}}(\aleph_K^*) \geqslant \Pi^{\mathrm{B}}(\aleph_{K+1}^*), \\
\text{(d)} & \Pi(\aleph_K^*) \geqslant \Pi^{\mathrm{B}}(\aleph_K^*, \boldsymbol{b}_K) \geqslant \Pi(\aleph^*), \\
\text{(e)} & \lim_{b_K \to 0} \Pi^{\mathrm{B}}(\aleph_K^*, \boldsymbol{b}_K) = \Pi(\aleph^*).
\end{array} \tag{38}$$

These results are proven in a straightforward manner. For example see [34].

Remark. In general one uses a series of weights, and stops at finitely small barrier, and finitely large, penalty values. There are a variety of minor variations to these types of approaches since their introduction in the late 1960s, but the essential idea has remained unchanged. For more details, the interested reader is referred to the exhaustive review in [31]. However, as a somewhat unelegant alternative to augmentations, one can also simply apply a brute force "pull back" into the feasible design space if the solution becomes infeasible.

B.3. An augmented objective

An exterior/interior augmented objective has the following form:

$$
\begin{aligned}
\Pi = & \underbrace{w_\kappa \left| \frac{\kappa^* - \kappa^{*\mathrm{D}}}{\kappa^{*\mathrm{D}}} \right|^{q_\kappa} + w_\mu \left| \frac{\mu^* - \mu^{*\mathrm{D}}}{\mu^{*\mathrm{D}}} \right|^{q_\mu}}_{\text{raw objective}} \\
& + \underbrace{\hat{b}_\kappa \left| \frac{\kappa_2 - \kappa_2^{\mathrm{crit}}}{\kappa_2^{\mathrm{crit}}} \right|^{-q_\kappa^{\mathrm{B}}} + \hat{b}_\mu \left| \frac{\mu_2 - \mu_2^{\mathrm{crit}}}{\mu_2^{\mathrm{crit}}} \right|^{-q_\mu^{\mathrm{B}}}}_{\text{moduli barriers}} \\
& + \underbrace{\hat{b}_s \left| \frac{s - s^{\mathrm{crit}}}{s^{\mathrm{crit}}} \right|^{-q_s^{\mathrm{B}}}}_{\text{shape barrier}} + \underbrace{\hat{b}_{\mathrm{AR}} \left| \frac{\mathrm{AR} - \mathrm{AR}^{\mathrm{crit}}}{\mathrm{AR}^{\mathrm{crit}}} \right|^{-q_{\mathrm{AR}}^{\mathrm{B}}}}_{\text{aspect ratio barrier}} + \underbrace{\hat{b}_{v_2} \left| \frac{v_2 - v_2^{\mathrm{crit}}}{v_2^{\mathrm{crit}}} \right|^{-q_{v_2}^{\mathrm{B}}}}_{\text{volume fraction barrier}} \\
& + \underbrace{\hat{p}_\kappa \left| \frac{\kappa_2 - \kappa_2^{\mathrm{crit}}}{\kappa_2^{\mathrm{crit}}} \right|^{q_\kappa^{\mathrm{P}}} + \hat{p}_\mu \left| \frac{\mu_2 - \mu_2^{\mathrm{crit}}}{\mu_2^{\mathrm{crit}}} \right|^{q_\mu^{\mathrm{P}}}}_{\text{moduli penalties}} \\
& + \underbrace{\hat{p}_s \left| \frac{s - s^{\mathrm{crit}}}{s^{\mathrm{crit}}} \right|^{q_s^{\mathrm{P}}}}_{\text{shape penalty}} + \underbrace{\hat{p}_{\mathrm{AR}} \left| \frac{\mathrm{AR} - \mathrm{AR}^{\mathrm{crit}}}{\mathrm{AR}^{\mathrm{crit}}} \right|^{q_{\mathrm{AR}}^{\mathrm{P}}}}_{\text{aspect ratio penalty}} + \underbrace{\hat{p}_{v_2} \left| \frac{v_2 - v_2^{\mathrm{crit}}}{v_2^{\mathrm{crit}}} \right|^{q_{v_2}^{\mathrm{P}}}}_{\text{volume fraction penalty}}
\end{aligned}
\tag{39}
$$

References

[1] V. Michaud, Liquid state processing, in: S. Suresh, A. Mortensen, A. Needleman (Eds.), Fundamentals of Metal Matrix Composites, 1992.

[2] C. Huet, Remarques sur l'assimilation d'un matériau hétérogéne á un milieu continu équivalent, in: C. Huet, A. Zaoui (Eds.), Rheological Behaviour and Structure of Materials, Presses ENPC, Paris, 1981, pp. 231–245.

[3] C. Huet, Universal conditions for assimilation of a heterogeneous material to an effective medium, Mech. Res. Commun. 9 (3) (1982) 165–170.

[4] C. Huet, On the definition and experimental determination of effective constitutive equations for heterogeneous materials, Mech. Res. Commun. 11 (3) (1984) 195–200.

[5] C. Huet, Application of variational concepts to size effects in elastic heterogeneous bodies, J. Mech. Phys. Solids. 38 (1990) 813–841.

[6] C. Huet, Hierarchies and bounds for size effects in heterogeneous bodies, in: G.A. Maugin (Ed.), Continuum Models and Discrete Systems, vol. 2, 1991, pp. 127–134.

[7] C. Huet, P. Navi, P.E. Roelfstra, A homogenization technique based on Hill's modification theorem, Continuum Models and Discrete Systems, 1991.

[8] C. Huet, in: P. Navi, A. Tolou (Eds.), Activities 1989–1996, Laboratory for Building Materials, Department of Materials Report, 1997.

[9] C. Huet, An integrated micromechanics and statistical continuum thermodynamics approach for studying the fracture behaviour of microcracked heterogeneous materials with delayed response, Engrg. Fract. Mech. (Special Issue) 58 (5–6) (1997) 59–556.

[10] C. Huet, Coupled size and boundary condition effects in viscoelastic heterogeneous bodies, Mech. Mater. 31 (12) (1999) 787–829.

[11] S. Hazanov, C. Huet, Order relationships for boundary conditions effect in heterogeneous bodies smaller than the representative volume, J. Mech. Phys. Solids 42 (1994) 1995–2011.

[12] S. Hazanov, M. Amieur, On overall properties of elastic heterogeneous bodies smaller than the representative volume, Int. J. Engrg. Sci. 33 (9) (1995) 1289–1301.

[13] M. Amieur, S. Hazanov, C. Huet, Numerical and experimental study of size and boundary conditions effects on the apparent properties of specimens not having the representative volume, in: C. Huet (Ed.), Micromechanics of Concrete and Cementitious Composite, 1993.

[14] M. Amieur, Etude numérique et expérimentale des effets d'échelle et de conditions aux limites sur des éprouvettes de béton n'ayant pas le volume représentatif, Doctoral dissertation No 1256, Ecole Polytechnique Fédérale de Lausanne, Lausanne, Switzerland, 1994.

[15] M. Amieur, S. Hazanov, C. Huet, Numerical and experimental assessment of the size and boundary conditions effects for the overall properties of granular composite bodies smaller than the representative volume, in: D.F. Parker, A.H. England (Eds.), IUTAM Symposium on Anisotropy, Inhomogeneity and Nonlinearity in Solid mechanics, Kluwer Academic Publishers, Dordrecht, The Netherlands, 1995, pp. 149–154.

[16] V.V. Jikov, S.M. Kozlov, O.A. Olenik, Homogenization of Differential Operators and Integral Functionals, Springer, Berlin, 1994.

[17] J. Aboudi, Mechanics of Composite Materials – A Unified Micromechanical Approach, Elsevier, Amsterdam, 1992, p. 29.
[18] T. Mura, Micromechanics of Defects in Solids, second ed., Kluwer Academic Publisher, Dordrecht, The Netherlands, 1993.
[19] S. Nemat-Nasser, M. Hori, Micromechanics: Overall Properties of Heterogeneous Solids, Elsevier, Amsterdam, 1999.
[20] W. Voigt, Über die Beziehung zwischen den beiden elastizitätskonstanten isotroper körper, Wied. Ann. 38 (1889) 573–587.
[21] A. Reuss, Berechnung der Fliessgrenze von Mischkristallen auf Grund der Plastizitätsbedingung für einkristalle, Z. Angew. Math. Mech. 9 (1929) 49–58.
[22] R. Hill, The elastic behaviour of a crystalline aggregate, Proc. Phys. Soc. (Lond.) A65 (1952) 349–354.
[23] J.D. Eshelby, The elastic field of an ellipsoidal inclusion, and related problems, Proc. Roy. Soc. A 241 (1957) 376–396.
[24] B. Budiansky, On the elastic moduli of some heterogeneous materials, J. Mech. Phys. Solids 13 (1965) 223–227.
[25] R. Hill, A self consistent mechanics of composite materials, J. Mech. Phys. Solids 13 (1965) 213–222.
[26] R. Christensen, A critical evaluation for a class of micromechanics models, J. Mech. Phys. Solids 38 (3) (1990) 379–404.
[27] Z. Hashin, Analysis of composite materials: a survey, ASME J. Appl. Mech. 50 (1983) 481–505.
[28] R. Hill, Elastic properties of reinforced solids: some theoretical principles, J. Mech. Phys. Solids 11 (1963) 357–372.
[29] W.C. Davidon, Variable metric method for minimization, Research and development report, ANL-5990 (Ref.) US Atomic Energy Commission, Argonne National Laboratories, 1959.
[30] R. Fletcher, M.J.D. Powell, A rapidly convergent descent method for minimization, Comput. J. 7 (1963) 149–154.
[31] A.V. Fiacco, G.P. McCormick, Nonlinear Programming: Sequential Unconstrained Minimization Techniques, Wiley, New York, 1990.
[32] L. Davis, Handbook of Genetic Algorithms, Thompson Computer Press, 1991.
[33] P. Gill, W. Murray, M. Wright, Practical Optimization, Academic Press, New York, 1995.
[34] D. Luenberger, Introduction to Linear and Nonlinear Programming, Addison-Wesley, Menlo Park, 1974.
[35] T.I. Zohdi, P. Wriggers, Aspects of the computational testing of the mechanical properties of microheterogeneous material samples, Int. J. Numer. Methods Engrg. 50 (2001) 2573–2599.
[36] A.A. Zhigljavsky, Theory of Global Random Search, Kluwer Academic Publishers, Dordrecht, The Netherlands, 1991.
[37] R. Horst, H. Tuy, Global Optimization-deterministic Approaches, Springer, Berlin, 1996.
[38] T.I. Zohdi, P. Wriggers, A domain decomposition method for bodies with microstructure based upon material regularization, Int. J. Solids Struct. 36 (17) (1999) 2507–2526.